Self-consistent modeling of the large-scale distortions in the geomagnetic field during the 24–27 September 1998 major magnetic storm

Y. I. Feldstein,[1] A. E. Levitin,[1] J. U. Kozyra,[2] B. T. Tsurutani,[3] A. Prigancova,[4] L. Alperovich,[5] W. D. Gonzalez,[6] U. Mall,[7] I. I. Alexeev,[8] L. I. Gromova,[1] and L. A. Dremukhina[1]

Received 12 May 2004; revised 2 May 2005; accepted 13 July 2005; published 19 November 2005.

[1] A new self-consistent version of a time-dependent magnetospheric paraboloid model is presented and tested on the 24–27 September 1998 magnetic storm interval (minimum $Dst = -207$ nT). The model uses DMSP satellite data to identify the location of the inner boundary of the magnetotail current sheet and the magnetic flux in the lobes and their variations with time. These inputs plus upstream solar wind dynamic pressure and IMF B_z values are used to iteratively model the Earth's field during the storm. Several interesting results with important consequences are obtained: (1) the model tail field strength at the Earth's surface (DT = −134 nT) is a significant fraction of the ring current value (DR = −167 nT); (2) the movement of the tail current sheet inward to $L = 3.5–4.0$ at storm maximum is consistent with geosynchronous magnetic field data; (3) at the Earth's surface the Chapman-Ferraro magnetopause current field (DCF = 117 nT) is almost equal at storm maximum to the value from the tail current, thus the fields from the two systems nearly cancel; (4) the magnetic flux from the polar cap in the course of the magnetic storm main phase approximately doubles in comparison with the magneto-quiet interval just before the storm onset; this fact shows that the driven processes prevail over dissipation processes throughout the storm main phase; (5) the large-scale internal currents in the magnetosphere (ring current, field-aligned currents, and magnetotail current) have significant influence on the shape and size of the magnetosphere; the location of the magnetopause subsolar point is different from that obtained by extrapolation of empirical results taken during high geomagnetic activity intervals and from magnetospheric models that do not include feedback from internal magnetospheric currents.

Citation: Feldstein, Y. I., et al. (2005), Self-consistent modeling of the large-scale distortions in the geomagnetic field during the 24–27 September 1998 major magnetic storm, *J. Geophys. Res.*, *110*, A11214, doi:10.1029/2004JA010584.

1. Introduction

[2] Models of the geomagnetic field in the magnetosphere are the basis for numerous studies of the energetics, topology, and dynamics of the large-scale structure of the magnetosphere. Because of both the significance of such field models and the versatility of their applications, the choice of a proper model is exceptionally important. Models must be verified by comparisons with observations. These comparisons reveal geophysical conditions, under which some models describe magnetic fields in the magnetosphere more precisely than others.

[3] The investigation of magnetic field variations and their structure in the inner magnetosphere during magnetic storms is becoming most intriguing. The drifts of energetic particles within this region produce intense ring currents leading to a significant deformation of the dipole geomagnetic field. Storm time radiation belts are formed. Charged particles that make up the radiation belts are energized, and then this energy is dissipated in the upper atmosphere. Dynamical models that more accurately describe the inner magnetosphere, especially during stormy periods, are needed in view of ongoing rapid expansion of human activities into near-Earth space. When constructing dynam-

[1] Institute of Terrestrial Magnetism, Ionosphere and Radio Wave Propagation, Troitsk, Russia.
[2] Space Physics Research Laboratory, University of Michigan, Ann Arbor, Michigan, USA.
[3] Jet Propulsion Laboratory, Pasadena, California, USA.
[4] Geophysical Institute, Slovak Academy of Sciences, Bratislava, Slovakia.
[5] Department of Geophysics and Planetary Sciences, Tel Aviv University, Tel Aviv, Israel.
[6] Istituto de Pesquisas Especiais, Sao Jose dos Campos, Sao Paulo, Brazil.
[7] Max Planck Institute for Aeronomy, Katlenburg-Lindau, Germany.
[8] Institute of Nuclear Physics, Moscow University, Moscow, Russia.

0148-0227/05/2004JA010584

ical magnetic field models and calculating the energy budget for the magnetosphere and its basic structural parts for particular events, the set of parameters that define the characteristics of the magnetic field model should be based upon available observations. For example, the time-spatial features of the dynamical magnetic field model are directly associated with both the current intensities, which generate variability of this field, and the location of currents in the magnetosphere.

[4] The structure of the magnetic field in the magnetosphere depends substantially on the location and intensity of the magnetospheric tail current. The present understanding of the contribution of the tail currents to the near-Earth magnetic field during magnetic storms is discussed in three fundamental reviews. These reviews were prepared by teams of authors citing results presented at international scientific conferences held during recent years. *Gonzalez et al.* [1994] evaluated the contribution of different sources (ring current, magnetopause currents, induced currents in the solid Earth) to the *Dst* variation. They stated: ''Other possible contributions to *Dst* from additional currents (ionospheric, field-aligned, tail currents, etc.) have not been quantified as yet.'' In the extended review by *Kamide et al.* [1998], which covers a wide range of ideas regarding magnetic storms, the magnetotail currents as one of the sources of magnetic fields in the magnetosphere are not considered at all. During the magnetic storm, Kamide et al. estimate the *Dst* variation of the magnetic field but do not even mention the contribution of tail currents to the *Dst* field formation. The review by *Daglis et al.* [2003] is the third of a series of storm-dynamics reviews preceded by *Gonzalez et al.* [1994] and *Kamide et al.* [1998]. It is only mentioned that during substorms the intensification of the near-Earth magnetotail current can modify the geomagnetic variations recorded at midlatitude observatories. The issue of the relative contribution of the fields of various magnetospheric sources to the inner magnetospheric field was also studied in detail by *Maltsev* [2004]. The views of different authors on the ring current effect in the storm time field depression are controversial. Actually, the estimates of the symmetric ring current contribution to *Dst* range from 0% to 40% and the contributions of the tail current and partial ring current vary from 25% to 80% and from 15% to 80%, respectively.

[5] The contribution of the magnetotail current system to the *Dst* variation during the main phase of magnetic storms has been consistently neglected. Variations of *Dst** (corrected *Dst* index) are described fully as the sum of the symmetric and asymmetric parts of the ring current field only.

[6] There is contradictory evidence regarding the contributions of various sources to the *Dst* variation of the geomagnetic field, which is the most important index for description of geomagnetic storm characteristics including intensity [*Alexeev et al.*, 1996; *Maltsev et al.*, 1996; *Turner et al.*, 2000; *Liemohn et al.*, 2001a, 2001b; *Kozyra et al.*, 2002]. It is usually believed now that *Dst* is a superposition of the magnetic fields due to the current on the magnetopause (DCF), ring current (DR), and magnetotail current (DT). The relative contribution of these sources to the *Dst* variation during the storm main phase is a topic for lively scientific discussions today. A range of different views on the importance of magnetotail currents has recently been expressed in the literature. *Alexeev et al.* [1996] and *Maltsev et al.* [1996] propose an approximately comparable contribution of DR and DT to the *Dst* variations. According to *Turner et al.* [2000] and *Baker et al.* [2001], there is only a 25% contribution of DT to *Dst* during magnetic storms. On the other hand, *Liemohn et al.* [2001a] and *Kozyra et al.* [2002] reported a strong agreement between modeled DR and observed *Dst* fields, which implies a minimal (even no) contribution of DT to *Dst* at the maximum of the storm main phase. Such a diversity of results is a consequence of using different magnetic field models, on one hand, and of using different methods to identify the boundary in the inner magnetosphere between the magnetotail current (which produces the DT contribution) and ring current (which produces the DR contribution), on the other hand. This inner boundary of the magnetotail current is located at 3.5–4.0 R_E [*Alexeev et al.*, 1996; *Maltsev et al.*, 1996], 6 R_E [*Turner et al.*, 2000], and outside of geosynchronous distance at 6.6 R_E [*Liemohn et al.*, 2001a, 2001b; *Kozyra et al.*, 2002]. In addition, there are differences in the representation of the ring current which contributes to magnetic field asymmetry and distortion in the inner magnetosphere. Models by Alexeev, Maltsev, and Tsyganenko 89, used by *Turner et al.* [2000], do not divide the inner magnetospheric current into separate parts as symmetric and asymmetric ring currents.

[7] In RAM model [*Liemohn et al.*, 2001a, 2001b; *Kozyra et al.*, 2002] during storm main phase when the convection electric field is strong, the bulk of the ring current ions are moving along open drift paths and therefore the main part of the energy in the ring current is contained in the partial ring current. During a storm recovery phase, when the convection weakens, open drift paths are converted to closed ones and the symmetric ring current develops.

[8] Modeling of the DCF, DR, and DT magnetic field during the 24–27 September 1998 magnetic storm and other storms (see Appendix A) is considered using a new self-consistent version of the PM model driven by appropriately-selected input parameters based on satellite observations. The following controversial issues will be examined: (1) How deep do tail currents penetrate into the inner magnetosphere during magnetic storms? (2) What is the role of tail currents in producing magnetic field distortions at geosynchronous orbit during a magnetic storm main phase? (3) What is the relationship (spatial and temporal) between the magnetotail and the ring current? (4) What are the consequences of closing the inner magnetotail currents through the dayside magnetopause on the magnitude of the magnetic field of the Chapman-Ferraro currents on the Earth's surface during the main phase of a storm?

2. Modeling of the DCF, DR, and DT Magnetic Fields Due to Current Systems in the Magnetosphere

2.1. Magnetospheric Magnetic Field

[9] The detailed description of the PM can be found in the works of *Alexeev et al.* [1996], *Alexeev and Feldstein*

[2001], and *Alexeev et al.* [2003]. The model has been named as paraboloid since the magnetopause, representing the paraboloid of revolution geometrically, is the essential element of the model. PM reflects both the physical and analytical description of the geomagnetic field within the whole magnetosphere. On the basis of physical ideas of the character of large-scale magnetospheric current systems and their magnetic fields, analytical relationships were obtained, which make it possible to calculate the geomagnetic field vector at any point in the magnetosphere as a function of input parameters of the model for magnetic storms of any intensity.

[10] The representation of the magnetic field in the modeling region is based on the modular principle, according to which the total magnetic field $B(t)$ is represented as the sum of contributions from major magnetospheric field sources (modules). Every module is an independent current system and each current system has its own intrinsic relaxation and inertia timescales. The magnetic field of each current system depending on its own input parameters is calculated separately. During the magnetic storm intervals the large-scale current systems are influenced not only by the current state of the interplanetary medium but also its time history during the previous hours. These effects, as well as the nonlinear character of the magnetospheric response to the extreme condition in the solar wind are taken into account in PM using model input parameters that specify the magnitude and evolution of important magnetospheric quantities. These input parameters are based on observed conditions in the magnetosphere during the entire course of the magnetospheric disturbances from magneto-quiet conditions to intense magnetic storms. Until recently, only a handful of empirical models of the large-scale magnetospheric magnetic field were available. These models were built on the basis of fitting satellite magnetic field measurements in the magnetosphere to various sets of approximating mathematical functions. PM uses physical notions of the possible character of the magnetospheric currents to select basis functions for these systems. For example, in contrast to the empirical models, the coefficients in the expansion of the potential for the magnetospheric magnetic field (B_T) due to the tail current system are determined on the basis of the $B_{TN} = 0$ (B_{TN} is the component of the magnetic field B_T normal to the magnetopause) condition, which indicates that in the PM the tail current system is not of a traditional sense. The traditional magnetotail current system closes the tail currents along the nightside magnetopause only. In contrast to this traditional presentation, in the PM the tail current system closes along the whole magnetopause, including its day sector. This is a key feature distinguishing PM from other magnetic field models, which has important consequences for the location of the magnetopause (since the inner part of the magnetotail current closes through the subsolar magnetopause) and for the contribution of magnetopause currents to *Dst*. For every magnetic field source, PM assumes a zero value of the normal component of the magnetic field on the magnetopause. The continuity equations for the magnetic field and electric current density, div $\mathbf{B} = 0$ and div $\mathbf{j} = 0$ in the magnetosphere outside the region of the current source location are valid as well.

[11] The total magnetic field vector B (x, y, z) for any point (x, y, z) in the magnetosphere in the solar-magnetospheric coordinate system and for the time t is

$$\mathrm{B}(t) = \mathrm{B_d}(\psi) + \mathrm{B_{CF}}(\psi, \mathrm{R1}) + \mathrm{B_T}(\psi, \mathrm{R1}, \mathrm{R2}, \Phi) + \mathrm{B_R}(\psi, \mathrm{b_r}) + \mathrm{B_{SR}}(\psi, \mathrm{b_r}, \mathrm{R1}) + \mathrm{B_{FAC}}(\psi, \mathrm{R1}, \mathrm{J_0}), \quad (1)$$

where:

B_d (ψ)	is the Earth's dipole field;
B_{CF} (ψ, R1)	is the field of currents on the magnetopause shielding the dipole field;
B_T (ψ, R1, R2, Φ)	is the field of the tail current system (cross-tail current and its closure magnetopause current);
B_R (ψ, b_r)	is the field of the ring current;
B_{SR} (ψ, b_r, R1)	is the field of currents on the magnetopause shielding the ring current field;
B_{FAC} (ψ, R1, J_0)	is the field due to field-aligned currents.

[12] The dipole field B_d is calculated as a gradient of the potential from Earth's internal sources using the IGRF-95 model with maximal order of harmonics 10. The B_{CF} field is found by solving the Neumann's problem used classic algorithm connected with solution of the Laplace equation for the potential U_{CF} ($\mathbf{B_{CF}} = -\mathrm{grad}\ U_{CF}$), with the boundary condition $\mathbf{B_{CF}} \times \mathbf{n} = -\mathbf{B_d} \times \mathbf{n}$, where $\mathbf{n}$ is the normal to the magnetopause.

[13] Magnetic field of the tail current system $\mathbf{B_T}$ is determined through the scalar potential U_t based on the relation $\mathbf{B_T} = -\ b_t\ \mathrm{R1}\ \mathrm{grad}\ U_t$, where $b_t = [2\Phi/(\pi \mathrm{R1}^2)]$ $[\mathrm{R1}/(\mathrm{R1} + 2\mathrm{R2})]$ is the magnetic field strength in the tail lobe at the inner boundary of the tail current sheet R2. The spherical harmonics and Bessel functions coefficients of expansion of the potentials U_{CF} and U_t are described by *Alexeev and Feldstein* [2001].

[14] For calculation of B_R, the magnetic field vector potential $\mathbf{A}$ ($\mathbf{B_R} = \mathbf{curl\ A}$) is introduced. The external boundary, outside which the ring current density is zero, coincides with the distance to the inner boundary R2 of the tail current sheet. The ring current density vector has only one azimuthal (longitudinal) component $-J_\varphi$ (r, θ, φ). The radial and latitudinal components of the current density vector are zero. Distribution of density J_φ in space is a function of the ring current magnetic moment, distance R2 and latitudinal angle θ. Shielding B_R currents at the magnetopause are calculated based on the requirement of zero normal component of the magnetopause magnetic field.

[15] For the B_{FAC} calculation the current system model by *Alexeev et al.* [2000] was used: the Region 1 field-aligned current system flows into the ionosphere along the polar cap boundary on the dawnside and flows out of the ionosphere at the duskside. The currents that close the circuit are located in the ionosphere and on the magnetopause.

2.2. PM Input Parameters

[16] Input model parameters are as follows: (1) date (year, day, UT), (2) coordinates of the point for calculation of the

magnetic field, (3) geomagnetic indices: *Dst*, *AL*, and solar wind parameters (n, V, B_z), (4) tilt angle of the geomagnetic dipole (Ψ), (5) geocentric distance to the magnetopause subsolar point (R1), (6) geocentric distance to the inner boundary of the current sheet in the magnetotail on the midnight meridian (R2), (7) magnetic flux in the magnetotail lobe (Φ), (8) magnetic field intensity of the magnetospheric ring current on the Earth's surface at the equator (b_r), (9) the total strength of the Region 1 FAC (J_0).

[17] The angle Ψ depends on time UT during a day and its ordinal number during a year; Ψ can be calculated using expressions given by *Alexeev et al.* [1996]. The R1 parameter is calculated from the balance between solar wind pressure at the magnetopause subsolar point $P\mathrm{sw} = 0.88\ \mathrm{nmV}^2$ and magnetic field pressure $B^2/2\mu_0$ where B is from (1).

[18] Input parameters of the PM, R2, and Φ, were determined using the *Vorobjev et al.* [2000] and *Starkov et al.* [2002] models based on DMSP electron and ion spectra taken every second, covering particle energies from 30 eV to 30 keV at about 900 km altitude. For the purposes of driving the PM model, the signatures of most interest are the low altitude signature of the earthward boundary of the tail current sheet and the polar cap area as an indicator of the strength of the magnetic flux in the magnetotail lobes.

[19] The poleward edge of the LLBL on the dayside and the b6 boundary (poleward extent of subvisual drizzle) on the midnight are used to identify the polar cap boundary. The LLBL poleward edge (LLBLpol) marks the boundary between closed and open (merging with IMF) field lines in the magnetosphere. The poleward boundary of soft electron precipitation on the nightside, identified as the b6 boundary, if the terminology of *Newell et al.* [1996] and *Feldstein and Galperin* [1996] is used, separates the region of auroral luminescence from polar rain.

[20] The angular radius θpc is calculated using the midnight colatitude values of the b6 boundaries (θb6) to mark the midnight edge of the polar cap and midday colatitude values of the LLBL boundaries (θllbl) to mark the dayside polar cap edge:

$$\theta\mathrm{pc} = (\theta\mathrm{b6} + \theta\mathrm{llbl})/2, \tag{2}$$

which means that the polar cap is approximated by a circle of a radius θpc. The circle centre shifts toward the nightside since $\theta\mathrm{llbl} < \theta\mathrm{b6}$.

[21] The tail lobe magnetic flux Φ, as an input PM parameter, is calculated based on the polar cap angular radius (θpc) using the relationship:

$$\Phi = 2\pi B_E R_E^2 (\sin\ \theta\mathrm{pc})^2, \tag{3}$$

where B_E and R_E are the dipole magnetic field at the Earth's equator and Earth's radius, respectively.

[22] Finally, the b2i boundary in the DMSP measurements [*Newell et al.*, 1996] is assumed to map to the inner boundary of the tail current sheet and can be used to determine the input parameter R2 in the present study. Here b2i marks the latitude where the energy flux of ions above 3 keV reaches maximum and approximately coincides with the transition between anisotropic and isotropic ion losscone distributions moving from low to high latitudes as observed by the NOAA-6 and NOAA-10 satellites [*Newell et al.*, 1998].

[23] The suprathermal plasma distribution in the equatorial night sector is characterized by the presence of the inner boundary of the central plasma sheet at which with decreasing radial distance a dramatic softening from several keV of the electron spectrum begins [*Fairfield and Vinas*, 1984], instead of a mean energy rise inward due to adiabatic acceleration of hot plasma with increasing magnetic field intensity. The region where such softening is observed is located between the inner boundary of the central plasma sheet and the plasmapause and was called Alfven layer or Remnant Layer, as plasma in this region is the remnant of magnetic activity, including the effects of earthward convection from the central plasma sheet. The thermal plasma drifts closest to the Earth and forms the inner (near-Earth) boundary of the Alfven layer, coincident with the plasmapause in steady-state conditions. This location marks the innermost penetration of magnetospheric plasma population at the inner edge of the Alfven layer. The mean energy of electrons in the Alfven layer decreases from several keV (at the inner boundary of the central plasma sheet) to several eV (at the plasmapause).

[24] A band of diffuse auroral emission and unstructured soft electron precipitation was discovered at low altitudes from ISIS-2 data equatorward from the auroral oval of discrete forms by *Lui and Anger* [1973]. The analysis of Dynamics Explorer (DE-1 and DE-2), AUREOL, DMSP, and Viking data has showed that electron energy in the region of unstructured soft electron precipitation increases monotonically with latitude increase [*Feldstein and Galperin*, 1993]. Electron energy spectra are practically the same above the ionosphere and in the conjugate equatorial plane of the inner magnetosphere [*Meng*, 1978]. The field-aligned electric fields are, as a rule, absent and the electron spectra are monotonic. The equatorward boundary of soft precipitation was first studied by *Galperin et al.* [1977] and *Gussenhoven et al.* [1981]. A close connection, or colocation, of this boundary with the plasmapause was demonstrated.

[25] *Newell et al.* [1996] offered automatic computer identification of plasma precipitation boundaries on the nightside based on DMSP satellite observations. Some of the identified electron boundaries of relevance to the present study are as follows: (1) b1e, a boundary of precipitation of the electrons with "zero" energy, corresponding to the boundary of convection that coincides with the plasmapause location; (2) b2e, the latitude λ, where $dE_e/d\lambda = 0$ (E_e is the average energy of the electrons). This latitude is a projection to ionosphere altitudes of the earthward boundary of the central plasma sheet.

[26] For the purpose of determining the value R2 needed by the PM, the location of the low-altitude signature of the onset of magnetotail stretching (b2i or b2e), when mapped to the equatorial plane along realistic stretched magnetic field lines, is taken to mark the location of the inner boundary of the magnetotail current. At near-midnight hours the near-Earth boundary of plasma sheet (b2e) is located very close to the isotropic ion boundary (b2i) [*Vorobjev et al.*, 2000].

[27] *Feldstein and Galperin* [1985, 1996] performed a detailed analysis of the relationship between electron precipitation structure at ionospheric altitudes and different plasma domains in the magnetosphere. They found that the equatorial boundary of soft auroral electron precipitation (see also references in the work of *Feldstein and Galperin* [1985, 1996]) is, according to low-altitude satellite data, coincident with the equatorward boundary of subvisual diffuse luminescence and is the plasmapause projection to ionospheric heights. *Galperin et al.* [1997] also examined the convection patterns measured by the Millstone Hill Radar in relation to the equatorward boundary of the soft diffuse electron precipitation in DMSP data (boundary b1e). They argue that b1e coincides with the inner boundary of the large-scale westward ion convection, i.e., with the instantaneous plasmapause. The low-energy electron boundary (b1e) has a clear geophysical meaning, both theoretically and experimentally, corresponding to the zero-energy Alfven layer and the instantaneous plasmapause location [*Nishida*, 1966; *Horwitz et al.*, 1986].

2.3. Indirect Estimation of Plasma Boundaries

[28] As noted earlier, R2 and Φ input parameters are determined using data on plasma precipitation boundaries observed by DMPS satellites. These observations are not continuous, the time step between successive orbits being $\sim$100 min. In addition, there are intervals of missing data due to various reasons, which creates a problem for the analysis. To overcome this difficulty, it was necessary to analytically express the dependence of boundary location on geomagnetic activity indices used to describe magnetic storms. The best geomagnetic activity indices for this purpose are *AL* and *Dst* indices because those reflect the magnetic field dynamics of basic storm elements, namely DCF, DR, and DT fields and westward electrojet (WE) intensity. The expressions needed were obtained for boundaries of plasma precipitation of various kinds [*Vorobjev et al.*, 2000; *Starkov et al.*, 2002]. The expressions for b2i, b2e, b6 (on the midnight), and LLBLpol (on the midday) boundaries are as follows:

for b2i,

$$\varphi = 66.46 + 0.005\,AL - 5.43 \times 10^{-7}\,AL^2 + 0.026\,Dst \quad (4)$$

for b2e,

$$\varphi = 66.66 + 0.009\,AL + 7.78 \times 10^{-7}\,AL^2 + 0.022\,Dst(5) \quad (5)$$

for b6,

$$\varphi = 71.82 - 0.0018\,AL + 0.0002\,Dst \quad (6)$$

for LLBLpol

$$\varphi = 80.08 + 0.0135\,AL + 4.52 \times 10^{-6}\,AL^2 + 0.038\,Dst. \quad (7)$$

The total field-aligned current J_0 of the Region 1 field-aligned current system according to *Alexeev et al.* [2000] is

$$J_0 = (1 + \cos\ \theta_{pc})\Sigma_p \Delta F_{pc} \quad (8)$$

and magnetic field at the subsolar point B_z is

$$B_z = \mu_0 \Sigma_p \Delta F_{pc} \sin\ \theta_{pc}/(2R1), \quad (9)$$

where $\mu_0 = 4\pi \times 10^{-7}$ H/m is the permeability of a vacuum, Σ_p = 10 S is height-integrated ionospheric Pedersen conductivity, ΔF_{pc} [kV] = $-11.5\ B_z$ [nT] + 33 and ΔF_{pc} is the potential drop across the polar cap according to *Papitashvili et al.* [1999] for $B_z < 0$. The relationships used to calculate the magnetic field components of the three-dimensional field-aligned current system can be found in the work of *Alexeev et al.* [2000].

[29] The ring current magnetic field intensity at the Earth's surface in the equatorial plane, DR, is the last input PM parameter. Usually, DR is determined from the total energy of ring current ions. However, this type of information is difficult or impossible to obtain for most magnetic storms. That is why in this analysis the *Dst* index is used to obtain the DR quantity. DR is obtained by subtracting the PM values of DCF and DT from the observed *Dst* at each time step. This approach that uses *Dst* to determine DR as an input PM parameter excludes the possibility of using the observed *Dst* variation to test the results of the modeling. For this study, testing will be carried out using independent magnetic field measurements, e.g., magnetic field data available from geosynchronous satellite.

3. Results of Magnetic Storm Modeling

3.1. Interplanetary Conditions During the 24–27 September 1998 Storm

[30] The 24–27 September 1998 magnetic storm was selected for analysis by the PM. A comprehensive set of observations and models are available in the literature for this storm as part of the Geospace Environment Modeling Inner Magnetosphere/Storms campaign, including results from a kinetic ring current model [*Liemohn et al.*, 2001b] for comparison to the PM.

[31] To briefly describe the storm development, the hourly values of the interplanetary medium parameters, IMF B_z and P (solar wind pressure), are shown in Figure 1 along with geomagnetic activity indices *AL* and *Dst* during the magnetic storm. A fast forward shock occurred at $\sim$2320 UT on 24 September. The solar wind speed increased from $\sim$450 km/s to $\sim$650 km/s and then gradually enhanced up to $\sim$800 km/s at $\sim$0400 UT 25 September, $|B|$ increased from $\sim$14 nT to $\sim$40 nT, N increased from $\sim$8 cm^{-3} to $\sim$27 cm^{-3}, and Ti increased from 3×10^5 K to 1.3×10^6 K. Upstream of the shock $B_z \sim -1$ to ~ -2 nT. The magnetic storm starts at 0000 UT 25 September, which is confirmed by a sharp increase of the *Dst* from -37 nT to -4 nT. This increase is due to the jump of the solar wind dynamic pressure from 3.8 nPa to 15.0 nPa. The IMF turning to the south occurs an hour later than the abrupt compression of the magnetosphere. The B_z component intensity reaches its maximum value of -17.9 nT at 0200 UT 25 September and remained negative (~ -12 nT) to 0600 UT. This caused the main phase of the magnetic storm as noted in *Dst*. At $\sim$0600 UT 25 September, there is a high-density plasma plug with N $\sim$18 cm^{-3} separating the sheath (Ti $\sim 5.8 \times 10^5$ K) from a magnetic cloud. Coincident with the plug is a short IMF B_z northward turning. An intense substorm

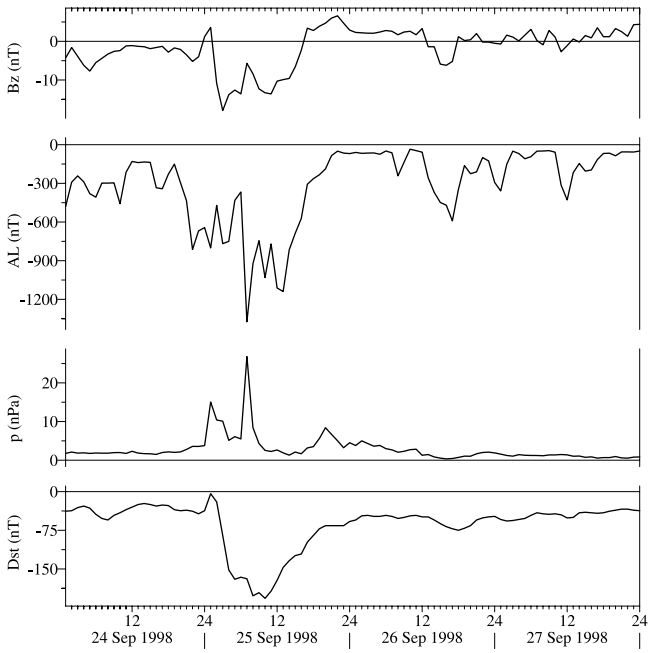

Figure 1. Variations of interplanetary medium parameters and geomagnetic indices used for the calculation of PM input parameters, including the IMF component B_z, dynamic pressure P, AL index, and the Dst index during the 24–27 September 1998 magnetic storm.

occurs at this time. A small recovery of the uncorrected Dst is also coincident with this event. The high-density region could possibly be a loop ahead of the CME dark matter.

[32] A magnetic cloud onset occurs at ~0710 UT 25 September. According to the Dst index the storm main phase lasts until 0900 UT, when a minimum Dst value of −207 nT is reached. The recovery phase starts with a rapid recovery of Dst to −66 nT by 1900 UT 25 September. This is followed by the substantially slower recovery of Dst to −36 nT at 2200 UT 27 September. During this slower recovery, sporadic magnetic disturbances in the auroral zone seen in the AL index also contributed to the Dst variation (Figure 1). At the storm main phase B_z reached ~−13 nT (by 0900 UT 25 September) and then turns to the north, with a corresponding attenuation of magnetic disturbances seen in the AL index.

[33] B_s (southward IMF) rotated through zero at 1500 UT and the cloud ended at ~1630 UT on 26 September. The plasma beta increased from 0.4 to ~1.0 at this time. From 1800 UT 26 September through 27 September, there are Alfven waves with $B_s \sim 4$ nT.

3.2. Estimation of the PM Input Parameters

[34] In Figure 2 the PM input parameters (R1, R2, Φ, DR, and J_0) are shown. The R1 parameter, geocentric distance to the subsolar point, is calculated in several ways. When the balance between solar wind and magnetic field pressures at the magnetopause subsolar point is used the profile (solid line) is obtained. The dotted line in Figure 2 designates R1 calculated as a function of the plasma pressure of the solar wind and the IMF B_z component according to expressions obtained by *Shue et al.* [1997]. Before the magnetic storm R1 ~ 10 R_E and at its beginning decreases to R1 ~ 7.1 R_E, reaching ~6.3 R_E at the main phase maximum. During the late recovery phase the R1 value is ~11 R_E.

[35] The differences between values of R1 from *Shue et al.* [1997] and geocentric distances from pressure balance in the PM (top panel, solid line) are ~ several tenths of R_E during most of the storm. These differences reach ~1 R_E for only some hours during the main phase of the storm. This means that the R1 by *Shue et al.* [1997] (dotted line) characterize conditions near the subsolar magnetopause point where there is the balance of pressures. Dashed line in Figure 2 marks R1-2 values, which were obtained based on pressure balance between the solar wind and the dipole magnetic field. R1-2 values systematically exceed R1 values by 0.5 R_E. However, when solar wind dynamic pressure decreases, this difference reaches 1.2 R_E.

[36] The R2 values (Figure 2, second panel) calculated on the basis of the b2i and b2e projection along magnetic field lines to the equatorial plane show only slight differences. Values of R2-2e (dotted line) practically repeat variations of R2-2i (solid line), but during separate intervals can differ up to 0.5 R_E nearer to the Earth. R2-2i or R2-2e is intended to be the real inner boundary of the tail current at midnight. The R2-2i values are adopted as the PM input parameter R2 shown in Figure 2. Both profiles R2-2i and R2-2e display the R2 distance shift from 5–6 R_E before the storm

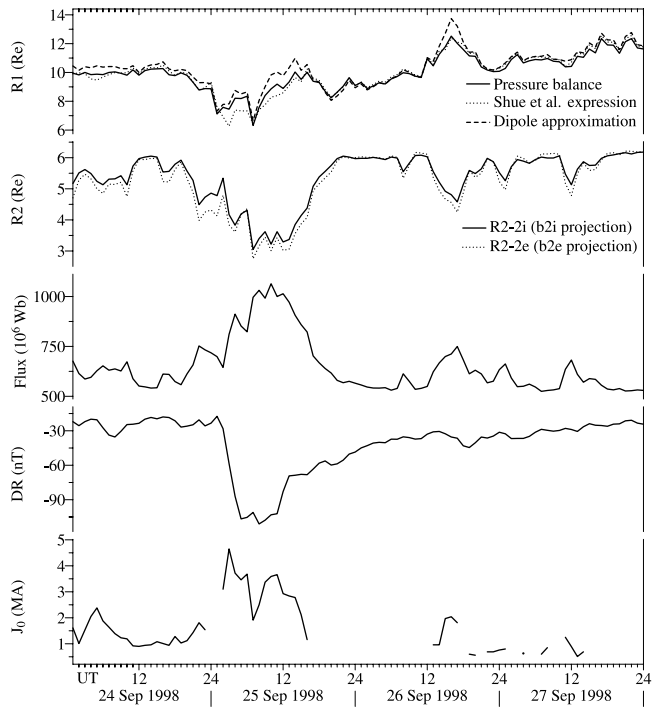

Figure 2. PM input parameters: (top) magnetopause stand-off distance R1 (solid line for the PM; dotted line for *Shue et al.* [1997], and dashed line for the dipole magnetic field); (second panel) distance to the tail current sheet inner boundary R2 (i.e., solid line for R2-2i using b2i, dotted line for R2-2e using b2e); (third panel) magnetic flux through the tail lobe Φ; (fourth panel) ring current field intensity DR on the Earth's surface calculated from Dst and magnetospheric sources; (bottom) total intensity of the Region 1 field-aligned current J_0.

to 3–4 R_E during the storm main phase and then reached the initial value during the storm recovery phase.

[37] As seen in Figure 2, the magnetic flux in the tail lobe Φ is $\sim 5 \times 10^8$ Wb before the magnetic storm, increases to 1.1×10^9 Wb mainly in connection with the equatorward shift of the midday LLBL polar boundary at the main phase maximum (0600–0800 UT 25 September), and then decreases (at the beginning quickly) to the value $\Phi \sim 5 \times 10^8$ Wb. This value persists during the remainder of the storm recovery phase on 26–27 September. This indicates that energy being dissipated in the magnetotail during these disturbed periods is derived not only from that accumulated in tail lobes before but also from solar wind energy continuously being loaded into the magnetotail during the main phase of the magnetic storm. Decrease of the magnetic flux in the magnetospheric tail is characterized by the poleward shift of the midnight polar cap boundary b6. This decrease only partially balances the increase of the magnetic flux due to its transfer from the dayside to the nightside. The fact that the magnetic flux transported into the lobe is approximately 2 times greater during the disturbed interval than during the quiet period shows that the magnetosphere is driven throughout the storm main phase [*Akasofu*, 2002]. Unloading processes prevail during the storm recovery phase.

[38] The development of the storm described by DR (Figure 2, fourth panel) shows that R1, R2, and Φ change abruptly during the storm main phase, which occurs also for J_0 (bottom panel). Total field-aligned current intensities $J_0 >$ 0.5 MA, calculated using equation (7), appeared throughout the storm interval. During the storm main phase, a maximum $J_0 \sim 4.5$ MA is reached. This is several times less than the intensity of Region 2 FACs calculated by *Liemohn et al.* [2001a] for the same storm, which were unrealistically large due to the use of a dipolar magnetic field. The calculation of R2 and Φ parameters is based on ionospheric measurements.

3.2.1. R1 and R2 Estimates

[39] The iteration approach is used to estimate R1. The first value of the input parameter R1 [R1(1)] is defined through a balance between solar wind pressure and magnetic field pressure near the magnetopause subsolar point for the total magnetic field B that is a sum of the dipole magnetic field and the magnetic fields of its shielding currents. The second value R1(2) is defined through the balance between the pressure of the solar wind and the pressure of the magnetic field, that being obtained on the basis of the PM. Iterations continue until the difference between two consequent values R1(N) − R1(N − 1) is less than 0.1 R_E. This process is shown as the double-sided arrow in the scheme of the magnetospheric magnetic field calculation (section 3.3).

[40] In this study, the mapped geocentric distance of the isotropy boundary (equation (4)) obtained after some iterations using the magnetic field configuration from the PM model (thereafter called R2-2i) was adopted as the location of the inner boundary of the current sheet in the equatorial plane. The first b2i mapping is along the dipole magnetic field line. This R2(1) value is used to calculate magnetic fields due to external sources in the PM. The second mapping of the b2i boundary is made along the magnetic field lines in the PM which takes into account the magnetic fields due to external sources. The new value of R2 is again used for calculation of the magnetic fields due to external current systems. This iteration continues until the difference between the two values R2(N) − R2(N − 1) is less then 0.2 R_E and this value is then adopted as R2-2.

[41] As mentioned above, R2-2i is used in our PM model. Shown in Figure 3 the R2-2i profile is compared with R2dip and R2-b profiles where R2-b is the trapping boundary described below. Differences between the R2 values obtained in the case of the dipole and PM mapping are within 1 R_E in general and decrease to 0.5 R_E during the storm main phase. The R2-2i values correspond to greater radial distances from the Earth than R2dip due to nightside magnetic field line stretching in the antisunward direction in the PM model. This stretching occurs down to relatively low L values.

[42] Another estimate of the boundary separating the ring and magnetotail currents is given by the trapping boundary (R2-b) taken to mark the outer edge of the symmetric ring current. Earthward of the trapping boundary closed drift trajectories do not encounter the magnetopause and high energy ions are stable trapped. Estimates of the trapping boundary location are based on an idealized model of high-energy particle motion in the geomagnetic field in the case where electric-field-associated particle drifts are small compared to magnetic field gradient and curvature drifts.

[43] The R2-b boundary is determined by considering the topology of magnetic field intensity isolines which divide the magnetosphere into two regions, an inner and an outer one. In the inner one magnetic field intensity B isolines in the magnetospheric equatorial plane produce closed quasi-circles around the Earth. In the outer one the lines B = const reach the magnetopause. The outer boundary of the inner region in the equatorial plane on the night side is located at distance R2-b, which can be approximated by the radial distance where the magnetic field at midnight has the same value as the magnetic field at the magnetopause subsolar point. The inner magnetosphere earthward of R2-b is a stable trapping region whose boundary is called the trapping boundary. Figure 3 shows a comparison between the estimated trapping boundary (R2-b) and R2-2i (the inner edge of the magnetotail current).

[44] The trapping boundary is located at geocentric distance of R2-b $\sim$ (6–7) R_E before the storm main phase and shifts to R2-b $\sim$ 4 R_E during the main phase. Then during the recovery phase it again retreats back to R2-b $\sim$ 8 R_E. The geocentric distance R2-b is less than R1 because of the greater (with regard to the dipole field) magnetic field intensity on the dayside (DCF influence) and the lowest value on the nightside (DT influence).

[45] Owing to the electric field from dawn to dusk in the nightside magnetosphere the R2-b boundary becomes shifted earthward by (0.5–2.0) R_E. The shifting is less during the main phase, when the night boundary is located at smaller distances from the Earth, and increases during the recovery phase, when the night boundary is located at greater distances from the Earth.

[46] Both the partial ring current and the innermost part of the magnetotail current are located near the plasma sheet inner boundary. The main difference in topology between the magnetotail and partial ring currents is that the partial ring current closes through the ionosphere and the tail

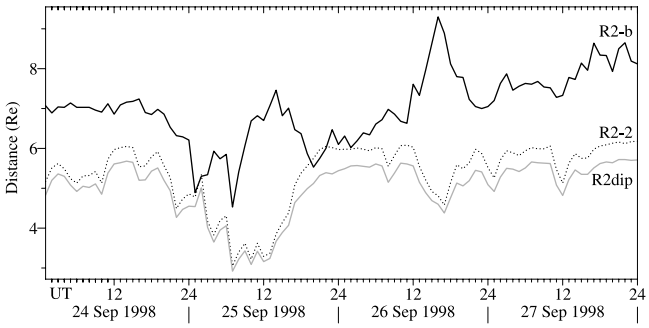

Figure 3. The comparison of the R2 boundary location calculated using PM (R2-2) with the R2 boundary location calculated by b2i mapping along the dipolar magnetic field line (R2dip) and the geocentric distance along the midnight anti-solar direction where the magnetic field intensity is equal to the magnetic field at the subsolar point (R2-b).

current closes through the magnetopause. There are regions in the inner magnetosphere where a portion of the current closes through the ionosphere and a portion continues moving outward until it encounters the magnetopause and closes. This ambiguity may contribute to the discrepancy in estimate of the relative contributions of magnetotail and partial/symmetric ring current to the *Dst* index during storms.

[47] During the storm main phase the transition between magnetotail-like currents and the partial/symmetric ring current is difficult to define. The partial/symmetric ring current (partially) and the magnetotail currents (fully) are both associated with the plasma sheet, the former closing through the ionosphere, the latter through the magnetopause boundary layer. Both produce stretching of the magnetic field in the inner region. The R2-2 boundary is located closer to the Earth, than R2-b. However, even the idealized boundary, the R2-b, is shifted far inward of the geosynchronous orbit during the storm main phase and it is located outside of this orbit during the recovery phase. In this paper, the inner edge of the magnetotail current is assumed to be given by the R2-2i boundary.

[48] The corrected geomagnetic latitude of the midnight current sheet (plasma sheet) inner boundary b2i (b2e) estimated using equations (4) or (5) can be seen in Figure 4. The locations of the boundaries are given at ionospheric altitudes. Before the magnetic storm and during the final stage of the recovery phase, b2i is located at magnetic latitude of $\sim$65° or $\sim$66° and moves equatorward to 56° at main phase maximum. The locations of b2i and b2e boundaries at midnight for low magnetic disturbance levels are practically coincide. At main phase maximum b2e moves equatorward to corrected geomagnetic latitude 53°. In Figure 4 the top profile shows the b6 boundary location during the storm. To estimate the magnetic flux Φ from the polar cap, b6 data are used.

3.2.2. Magnetic Flux Φ Estimation

[49] The relations (2) and (3) used for calculating the input parameter Φ (magnetic flux into the tail lobe) requires knowledge of not only the b6 plasma boundary but also LLBLpol. Their variations during the storm, parameterized by the *AL* and *Dst* indices, are shown in Figure 4 and Figure 5. The comparison of empirical data on plasma precipitation boundaries (namely LLBLpol and 2bi) with observed (DMSP) data is presented in Appendix A (subsection A1.3).

[50] On the nightside the polar cap boundary b6 is shifted at midnight rather insignificantly to the pole (MLAT $\sim$ 74°) when storm main phase takes place. In the remaining time during the storm, b6 is fixed at MLAT $\sim$ 72°. The midday boundary of LLBLpol is located at $\sim$78° before the storm. At the main phase maximum, it shifts to MLAT $\sim$ 64° and then comes back to $\sim$78° during the recovery phase.

[51] The motion of the LLBLpol to geomagnetic latitudes of $\sim$64° near noon MLT during the main phase of the 24–27 September 1998 event, is characteristic for other magnetic storms as well. *Meng* [1983, 1984] investigated the latitudinal variations of the near-noon sector of the polar cusp boundaries during three magnetic storms. It was found that the near-noon cusp equatorial boundary, which is simultaneously the LLBL polar boundary, shifts equatorward during the magnetic storm main phase in latitude by more than 10°. For $B_S \sim 15$ nT and $Dst \sim -150$ nT the equatorial cusp boundary is located at geomagnetic latitudes $\sim$64°. The polar-cusp-region shift toward the equator is more closely connected with the southward interplanetary magnetic field than with the *Dst* intensity variation.

[52] During of the storm main phase *Dst* minimum is accompanied by a very intense substorm at 0600–0800 UT with hourly mean index AL ~ -1500 nT at 0600–0700 UT on 25 September (see Figure 1). The magnetic flux from the polar cap reaches its maximum during this substorm with hourly peak value $\sim 1.06 \times 10^9$ Wb and decreases after the end of the substorm, which coincides with the onset of the storm recovery phase. Decrease of the magnetic flux has monotonic character in the northern hemisphere and is characterized by a leap-like increase to $\sim 1.7 \times 10^9$ Wb in the southern hemisphere. A relative minimum in Φ values was registered at 1200–1300 UT. This was several hours after the end of the intense substorm at 0600–0800 UT and therefore the decrease of the polar cap magnetic flux can not be associated with this substorm.

[53] Increase of the polar cap magnetic flux at the onset of a substorm active period with its subsequent decrease is described by *Frank et al.* [1998]. The intense substorm at 0630 UT on 25 September 1998 is characterized by a

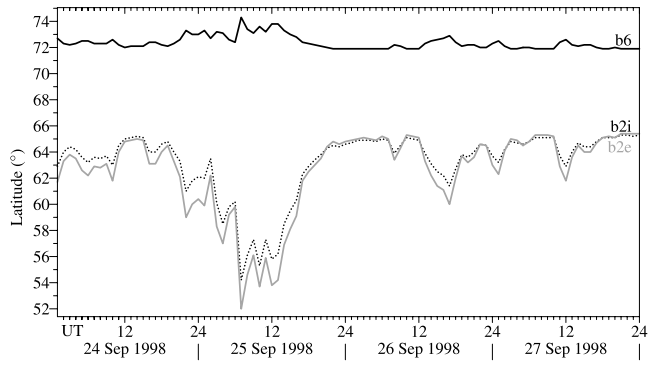

Figure 4. The variation of the location of the b2i, b2e, and b6 boundaries in the midnight sector during the magnetic storm.

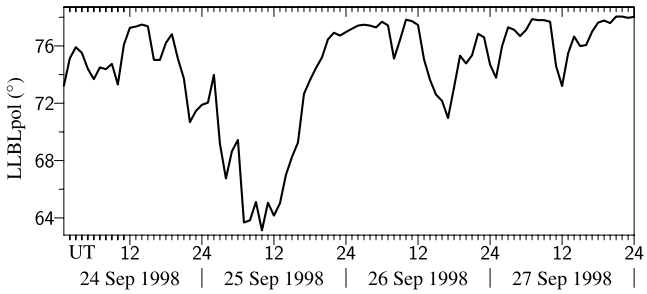

Figure 5. The corrected geomagnetic latitude of the LLBL poleward boundary LLBLpol variations in the near-noon sector during the 24–27 September 1998 magnetic storm.

decrease of 9% in the polar cap magnetic flux before the substorm followed by a 25% increase during the substorm. Sporadic magnetic disturbances during the storm recovery phase on 26–27 September are accompanied by magnetic flux increases in the tail lobe. However, one should bear in mind that the description of the magnetic flux variations in the course of substorms based on hourly values is relatively rough.

[54] *Borovsky et al.* [1998] note that substorms occurring during magnetic storms are accompanied by dipolarization at the substorm onset. However, the reduction in the magnetic field line orientation is typically small compared with the actual field line deviation from the dipole configuration. Hence a substorm dipolarization does not relax the nightside magnetic field configuration to a dipole-like one.

[55] *Ostapenko and Maltsev* [2000] carried out model calculations of fields in the inner magnetosphere and in the tail during magnetic disturbance intervals. The significant role of the magnetotail current for generation of *Dst* variations was shown.

[56] Results of the statistical study of magnetic field behavior during magnetic storms in the near- and midtail central plasma sheet are presented by *Schoedel et al.* [2002] based on Geotail observations. During magnetic storms with moderate $Dst \sim -85$ nT the magnetic field intensity increases from 13 nT during the magneto-quiet intervals to 28 nT during the storm main phase at geocentric distance 15 R_E. The corresponding values at geocentric distance 25 R_E are 7 nT and 13 nT. Values for the recovery phase range between those for the main phase and those for quiet times, being usually not significantly different from the latter. Hence magnetic field in the tail during the storm main phase does substantially increase with subsequent rapid return to its quiet level during a storm recovery phase. Magnetic flux variations in the tail for the 24–27 September 1998 magnetic storm correspond reasonably well to the statistical results obtained on the basis of averaging observations from 81 storms. *Skoug et al.* [2003] even suggest the dominant contribution of the tail current to *Dst* during the main phase of the 31 March 2001 superstorm.

[57] In addition, there are well-known geomagnetic activity equinoctial maxima. As a statistical study by *Newell et al.* [2002] shows, the polar cap is largest around the equinoxes, being smaller around solstices. It means that the magnetic flux in the tail lobes increases, not decreases, with the increase of the magnetic disturbance level.

[58] The magnetic flux intensity Φ in the tail lobe shown in Figure 2 was calculated as a function of *AL* and *Dst* for each hour UT. The corresponding relationships are obtained by means of statistical analysis of DMSP satellite data on plasma precipitation boundaries. The location of a plasma precipitation boundary using low-altitude DMSP satellite observations is determined only locally. Recently, a more global view of the polar cap boundary has become available based on auroral luminosity at ultraviolet wavelengths. Ultraviolet imagers (UVI) on board high-altitude satellites allow in principle the determination of the instantaneous location of auroral precipitation boundaries. However, discriminating the regions with diffuse and discrete precipitations from UVI data is difficult and usually particle instruments yield better estimates of the different plasma boundary locations.

[59] In Figure 6 the Φ profile is displayed from the statistical approach used in this study (red line). In addition, there were used the values Φ (DMSP + UVI) obtained by means of the OVATION procedure separately for the north and south polar caps for each UT hour and displayed for the northern (blue line) and southern (triangles) hemispheres. Breaks of the northern hemisphere profile mean absence of data. The leap-like Φ variations obtained from UVI data can be of geophysical nature, although it is likely that a significant portion of the difference is due to instrumental and algorithmic noise.

[60] A comparison of magnetic fluxes calculated by these two methods shows a general agreement in the absolute magnitude and in variations during the magnetic storm. For the storm main phase the magnetic flux in the northern hemisphere increases from $\sim 5 \times 10^8$ Wb in magneto-quiet interval about 1200 UT on 24 September 1998 to $\sim 1 \times 10^9$ Wb at 0600–0900 UT on 25 September and decreases again to $\sim 3 \times 10^8$ Wb during the magneto-quiet interval, i.e., for late hours on 27 September. During the

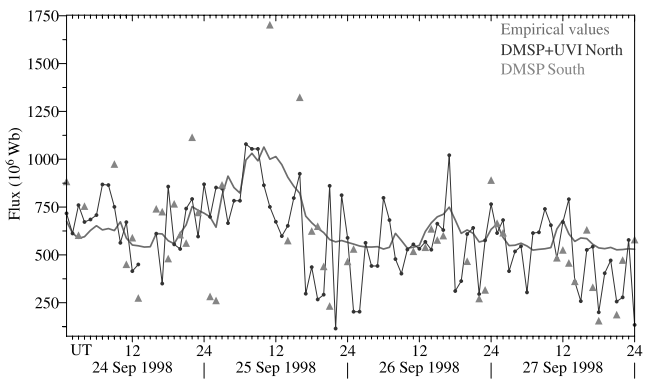

Figure 6. Variations of the magnetic flux from the polar cap calculated using empirical equations (2), (3), (6), and (7) (red line), the magnetic flux calculated using the POLAR UV photometer and DMSP particles measurements in the northern hemisphere (DMSP + UVI North: blue line), and DMSP particles measurements in the southern hemisphere (DMSP South: triangles) during the 24–27 September 1998 magnetic storm. The OVATION method is used to obtain the DMSP + UVI North and DMSP South values. See color version of this figure at back of this issue.

storm recovery phase, the magnetic flux from the polar cap increases leap-like during substorms at 1600 UT on 26 September and 1100 UT on 27 September (Figure 1). Differences in magnetic fluxes between Polar UVI and DMSP data range within the limits of the standard deviations.

[61] The polar cap boundary location based on the luminosity distribution is ambiguous. To some extent, it depends on the method used. *Craven and Frank* [1985] produced the first quantitative definition of auroral boundaries locations using a threshold approach for DE images. A similar threshold approach has been applied to Polar UVI images by *Brittnacher et al.* [1999]. *Kauristie et al.* [1999] compared the oval boundaries in Viking UVI images with simultaneous DMSP particle precipitation data in the midnight-evening sector. The results of this investigation indicate that caution is needed in using UV images to compute changes of the magnetic flux from the polar cap under different states of magnetic activity. *Baker et al.* [2000] determined the poleward auroral emissions boundaries from Polar UV images using both the threshold method and a ratio method. The investigation identified a systematic latitudinal difference between UVI and DMSP boundaries in the evening sector with a magnitude of about 1°.

[62] *Newell et al.* [2002] calibrated the locations of the auroral oval polar boundary incorporating different data sources: SuperDARN HF radar data, DMSP particle data, and Polar UVI images. As a calibration standard choice, DMSP particle boundaries were used. The convection reversal boundary observed by SuperDARN coincides with, or lies 1° equatorward, if compared with the DMSP polar boundary. The standard deviation is typically 1–2°. This is much better than the DMSP boundaries calibrations with Polar UVI. The standard deviations between the Polar UVI poleward boundary and the DMSP-determined poleward boundary range between 2.5° and 3.5°. This is just about double the standard deviations from SuperDARN. To estimate the error in the polar cap magnetic flux assuming that the polar cap during the magnetic storm main phase is circular with radius of 18° in colatitude and a given error in boundary location of about 3° is of interest. The error in the flux would be ~35%. The apparently systematic difference between the magnetic fluxes determined by two methods is associated with the difference in the dayside polar cap boundary location obtained by various methods. Precipitating particle data take into account a complex structure of dayside precipitations [*Newell and Meng*, 1994].

[63] Owing to more sophisticated automated fitting procedures, an alternative method for obtaining Φ values can be used for the events with available concurrent measurements of plasma boundary locations and auroral UV luminosity, which allows to identify the polar cap boundary [*Newell et al.*, 2001, 2002]. The procedure to determine various auroral oval parameters using complex ground-based and satellite observations and then to calculate the magnetic flux intensity in the lobe on the basis of the already known polar cap area OVATION (Oval Variation, Assessment, Tracking, Intensity, and Online Nowcasting) was proposed [*Newell et al.*, 2001, 2002].

3.2.3. DR Estimation

[64] Shown in Figure 2 the essential input parameter for the PM model is DR (ring current magnetic field intensity on the Earth's surface) calculated from the *Dst* variation. The intensity of the DR field on the Earth's surface is defined from the equation:

$$\mathrm{DR} = Dst - \mathrm{DT} - \mathrm{DCF}. \tag{10}$$

The magnetic field due to the ring current (DR) at the subsolar point was defined using the ring current magnetic moment M_{RC} as

$$\mathrm{B(DR)} = \mathrm{M_{RC}}/(\mathrm{R1})^3, \tag{11}$$

where M_{RC} is calculated from the expression [*Belova and Maltsev*, 1994]:

$$\mathrm{M_{RC}/Mdip} = (1/2)(\mathrm{B(DR)}/B_E)(R_{km}/R_E)^3, \tag{12}$$

where Mdip is the dipole magnetic moment, B_E is the dipole magnetic field and $B(DR)$ is the ring current magnetic fields at the Earth's equator, R_{km} is the geocentric distance to the external boundary of the ring current, i.e., the radius of a sphere, where the model ring current flows. The coefficient 1/2 takes into account the twofold increase of the field inside the sphere in comparison with the field outside the sphere. The calculations were made assuming the following values of R_{km}:

$$\begin{aligned} R_{km} &= 6\,R_E \text{ for } \mathrm{R2} \geq 6 \\ R_{km} &= \mathrm{R2} \text{ for } \mathrm{R2} \leq 6 \end{aligned} \tag{13}$$

It is worth noting that there is another way to obtain the value of DR using data on total ion energy ($1 \leq E \leq 300$ keV) in the magnetosphere.

3.3. Magnetic Fields of Different Current Systems

[65] The structure of the computational program and sequence of successive steps for estimation of the PM input parameters as well as intensities of DCF, DT, DR, and $\mathrm{D_{FAC}}$ current systems are presented in the scheme below. Magnetic fields of different current systems considered on the Earth's surface (including induction currents in the solid Earth with the induction coefficient 1.5 as well) are determined according to the proposed scheme (Figure 7) and plotted in Figure 8. PM model values of DCF, DT, and DR, as well as the observed *Dst* and derived *Dst** have not been corrected to remove the contribution of induction currents in this figure. DCF calculated from magnetopause currents in the PM is plotted (top panel, solid line). That can be compared with DCF profile (dotted line), DCF = 0.02 Vsw (km/s) [Nsw ($\mathrm{cm^{-3}}$)]$^{0.5}$ = 16 $\mathrm{P^{1/2}}$, P in nPa [*Burton et al.*, 1975]. These values are remarkably close to one another except during the interval of the main phase. The DCF - 16 $\mathrm{P^{1/2}}$ value before the storm onset on 24 September is ~7 nT, that at the late recovery phase on 27 September is ~0 nT. During the main phase magnetic fields of Chapman-Ferraro currents on the Earth's surface increase due to dayside magnetopause erosion and to the decrease of geocentric distance to the magnetopause. At 0600 UT on 25 September difference between intensities of the magnetic field in two model presentations of DCF increased up to 34 nT.

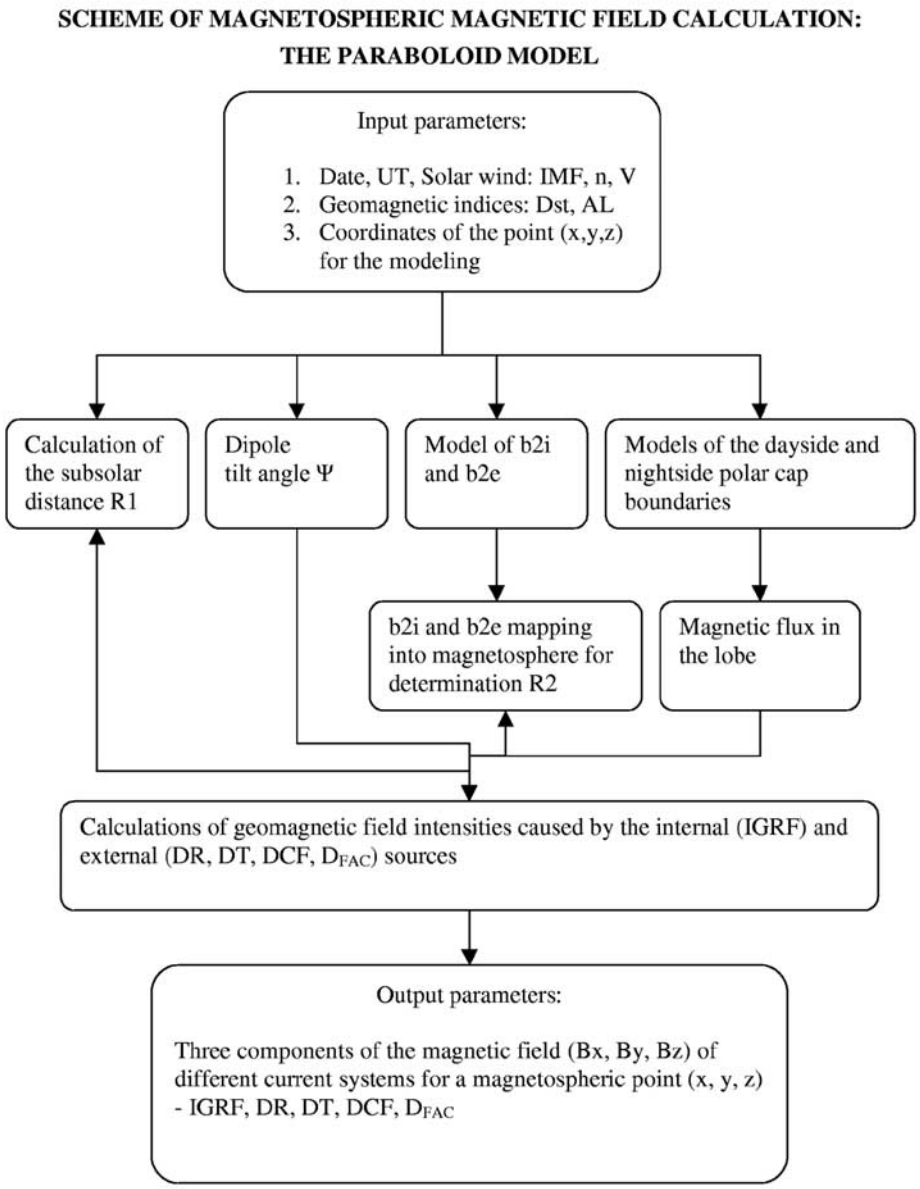

Figure 7. The scheme of magnetospheric magnetic field calculation using the PM.

[66] The bottom panel displays PM values of DT. The middle panel gives DR calculated by subtracting the PM model values of DCF (top) and DT (bottom) from the observed *Dst*. For comparison, there are also plotted *Dst* (dotted line) and *Dst** (shaded line). *Dst** is obtained by correcting the observed *Dst* for contribution from the magnetopause currents according to *Burton et al.* [1975]. *Dst** is usually assumed to be the contribution to the disturbance field from the ring current and for the September storm is also given by *Liemohn et al.* [2001b] with an additional correction to remove the diamagnetic effects of the solid Earth. The profiles DR in PM and *Dst* are in close agreement. Increases in negative DT in PM are largely balanced by corresponding increases in DCF leaving the value of DR $\sim$ *Dst*. Only during several hours at the culmination of the main phase *Dst* is approximately 40 nT less than DR.

[67] DR and *Dst** profiles differ by up to 100 nT during the storm main phase. The *Dst** profile in Figure 8 (if corrected for the diamagnetic currents in the Earth) is in close agreement with the ring current field, a sum of its symmetric and asymmetric parts, calculated based on the RAM model [*Liemohn et al.*, 2001b]. Such an agreement means that, in general, the magnetic field contributions to *Dst* from the ring current systems in the RAM and PM models differ during a storm main phase by the magnetic field contribution of the tail current system. During the storm main phase, DR fields in the RAM model are more intense than assumed in the PM. The magnetic field contribution of the ring currents in the RAM model may

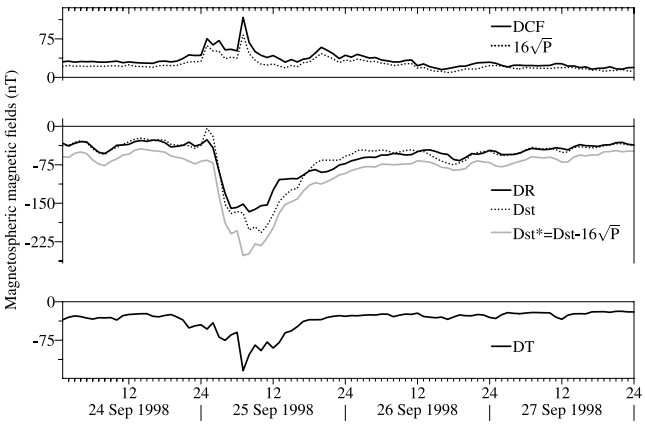

Figure 8. Variations of the magnetic fields on the Earth's surface including the fields of the induction currents in the solid Earth during the 24–27 September 1998 magnetic storm due to: (top) the magnetopause current DCF, according to PM (solid line), *Liemohn et al.* [2001b] (dashed line); (middle) ring current DR according to PM (—), where DR = *Dst* − DCF − DT, *Dst* (dashed line), $Dst^* = Dst - 16P^{1/2}$ (shaded line); (bottom) tail current DT.

be overestimated somewhat as a consequence of approximations used in this model to represent inner magnetospheric magnetic and electric fields. The RAM model [*Liemohn et al.*, 2001b] utilizes a modified [*McIlwain*, 1986] electric field model and a dipolar magnetic field. The *Dst** values calculated are somewhat smaller when a self-consistent electric field calculation is applied in a newer version of RAM. On the other hand, the PM model represents the symmetric portion of the ring current and asymmetric tail current.

[68] The use of a dipolar magnetic field approximation in the inner magnetosphere in the RAM model becomes less accurate as activity levels increase. During intervals of high magnetic activity the magnetic field in the inner magnetosphere loses its dipole configuration, field lines become stretched in the antisunward direction. In a tail-like magnetic field configuration ion drifts are directed to the plasma sheet central plane, instead of earthward. It leads to lower magnitudes of total ion energy in the inner magnetosphere and, respectively, a decrease of the ring current magnetic field contribution. The electric field in the magnetosphere is substantially more complex than its description in existing models [*Rowland and Wygant*, 1998; *Angelopoulos et al.*, 2002]. Subsequent improvement of the magnetospheric magnetic field model, including a more realistic ring current model, is a task for future efforts.

[69] As seen, the maximum depression of the magnetic field in PM due to DR and DT during the storm main phase is −167 nT and −134 nT, respectively, i.e., the ratio DT/DR = 0.80. During the storm recovery phase attenuation of magnetopause and magnetotail currents is more rapid than that of ring current. By 1600 UT 25 September, DT in PM recovered to −38 nT and then persisted at the level of −25 nT up to the end of recovery phase at 2300 UT 27 September. On the other hand, DR determined using PM values of DT and DCF recovered to −95 nT at 1600 UT on 25 September and then gradually reached −40 nT by the end of the recovery phase.

[70] The module describing the magnetic fields of the partial ring current system (PRCS) is absent in the PM. The tail current system directly adjoins the symmetric ring current on the nightside. As a result, the day-night asymmetry in the low-latitude magnetic field intensity is given by the magnetotail current system and the tail current field DT does partially contribute to the field usually ascribed to the partial ring current.

[71] In the PM along with the tail current enhancement during the storm main phase the earthward shifting of its boundary takes place. This produces an increase in the day-night asymmetry. A similar increase in the day-night asymmetry results from enhancing the PRC in some other magnetic field models.

4. Accuracy of the PM Model and Its Comparison With Other Models

4.1. PM Magnetic Field Versus GOES 8 Geosynchronous Data

[72] The PM model assumes a deep earthward penetration of the magnetotail current. To test this assumption, direct magnetic field measurements by the GOES 8 geosynchronous satellite are used. These observed data (hourly mean values of solar-magnetospheric B_x, B_y, B_z components and geomagnetic field magnitude B monitored by GOES 8) are compared with model profiles during the magnetic storm. For this purpose hourly mean values of the field magnitude B and its components B_x, B_y, B_z were determined along the trajectory of the GOES 8 geosynchronous satellite using the PM. The local geomagnetic midnight corresponds to 0500 UT. In Figure 9 the results of a comparison between PM values (dotted line) and observational data (solid line) are shown in solar-magnetospheric B_x, B_y, B_z components and geomagnetic field magnitude B along the GOES 8 trajectory. The corresponding correlation coefficients between model and observational values for each component range between 0.63 and 0.96, and mean quadratic deviations range between 14.1 nT and 22.9 nT. There is quite good agreement between model estimates and geosynchronous satellite measurements.

[73] Meanwhile, according to the GOES 8 geosynchronous satellite data (Figure 9) a significant change of the magnetic field orientation is seen in the nightside magnetosphere within the interval of the magnetic storm main phase. During quiet days the field components at local midnight are B_x = 30 nT, B_y = 0, B_z = 90 nT. At 0500 UT 25 September the changes of geomagnetic field components were ΔB_x = +130 nT, ΔB_y = 0, ΔB_z = −50 nT according to GOES 8 measurements. Thus while during quiet intervals the geomagnetic field at midnight along GOES 8 geosynchronous orbit was close to dipolar, within the magnetic storm main phase the field lines became stretched in the antisunward direction. The degree of field deformation at geosynchronous orbit is closely associated with the b2i boundary location [*Newell et al.*, 1998]. As reported, the correlation coefficient between magnetic field elevation angle (GOES 5 and GOES 7 data) and b2i boundary location derived from DMSP-6 and DMPS-8 measurements was 0.84. When the b2i boundary is located at geomagnetic

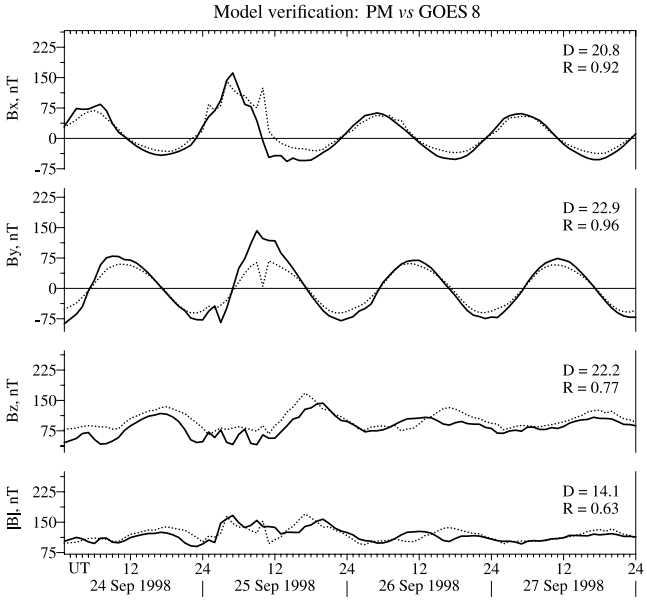

Figure 9. PM modeling of the 24–27 September 1998 magnetic storm. The comparison of measured (solid line) and modeled (dotted line) magnetic fields along the GOES-8 orbit: B_x GSM, B_y GSM, B_z GSM and total $|B|$ (from the top to the bottom).

latitude ~70°, the elevation angle is ~50°; for a boundary at ~60°, the elevation angle is ~0°. This means that when the level of magnetic disturbance increases (MLAT is more equatorward), magnetic field lines become more and more stretched into the magnetotail. Under magnetic storm conditions (b2i latitude of ~60°) magnetic field lines finally acquire the antisunward direction at geosynchronous orbit.

[74] Additional modeling was performed to determine the influence of varying the parameter R2 on the agreement between the results of PM and geosynchronous magnetic data. For an interval during the main phase of the magnetic storm from 2100 UT 24 September to 1600 UT 25 September 1998, when R2 is assumed to be ~4.0 R_E, magnetic field components B_x, B_y, B_z in GSM coordinates and total B (those measured by GOES 8) were calculated for different values of the R2 parameter. Figure 10 presents the observational values (solid line) and results of modeling for R2 = R2-2i (PM, dotted line), R2 = R2-2i + 3 Re (shaded line), R2 = R2-2i + 6 Re (dashed line). It is evident that for larger values of R2 the agreement between GOES 8 and PM degrades. This provides observational support for the movement of the tail current sheet to low L values during the storm main phase, namely as low as R2–2 ~ 4.0 R_E.

[75] Moreover, variations of the magnetic field B_x GSM and B_z GSM components monitored at geosynchronous orbit during the magnetic storm main phase (ΔB_x GSM $\gg$ 0; ΔB_z GSM < 0) give evidence of the shift of the tail current system boundary toward L < 6.6 during the storm main phase. Magnetic field lines at geosynchronous orbit are stretching in the antisolar direction as the tail current sheet inner boundary approaches the Earth. Change of magnetic field character and appearance of magnetospheric tail currents at geosynchronous orbit and nearer to the Earth at a storm main phase should be taken into account in ring current models. Moreover, in Appendix A some additional results from the PM and their comparison with both the GOES data and *Dst* variations are presented and discussed.

4.2. Modeling of the Global Geomagnetic Field

[76] The dynamics of magnetospheric plasma domains is not fully understood, particularly during magnetic storms. The mechanisms by which energy and matter are transferred from the solar wind to the magnetosphere and from one region to another are not completely known. It leads to the existence of many models, which describe the configuration and magnetic fields of large-scale current systems in the magnetosphere.

4.2.1. On Some Magnetospheric Magnetic Field Models

[77] For sake of transparency, one can divide the recently available models of external sources into empirical and hybrid. Empirical models were built by adjusting the observational data to a set of approximating functions in order to reach the best fitting for as much data as possible. Empirical models set up their current systems to yield reasonable average conditions of the magnetosphere. Some of these models even allow a choice of the level of activity. In some of these models (unlike the PM), the dependence of modeling results on the location of observed boundaries is absent. A comparison of the PM to some magnetic field models at geosynchronous orbit is necessary to provide the reader with an understanding of the main features of existing magnetic field models relative to the features in the PM. Hybrid models fit observations to basis functions chosen to be consistent with physical notions about the character and magnetic fields of magnetospheric large-scale current systems. In some of them the characteristic bound-

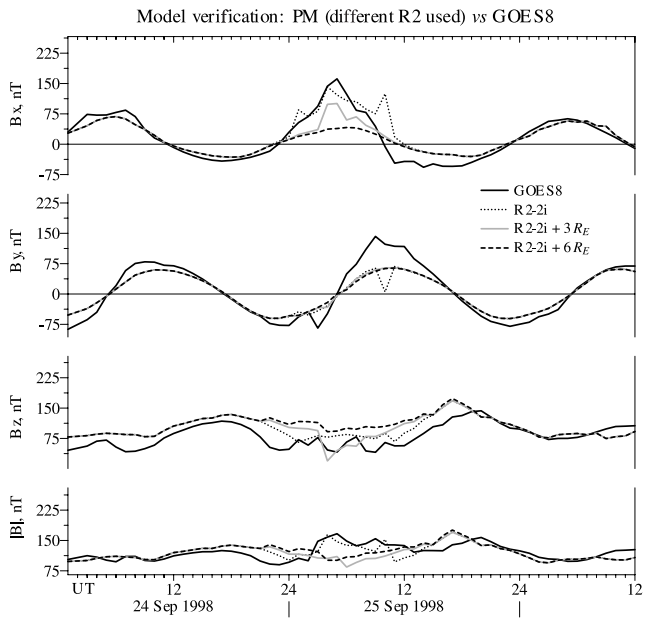

Figure 10. GOES 8 magnetic field observations (solid line) and PM modeled magnetic field components at geosynchronous orbit during the main phase of the 24–27 September 1998 magnetic storm for different R2 values: R2 = R2-2i (dotted line), R2 = R2-2i + 3 R_E (shaded line), and R2 = R2-2i + 6 R_E (dashed line).

aries of plasma domains and their dynamics are used explicitly.

[78] A few magnetic field models, which were used or are in use today are (1) MF, the Mead and Fairfield model [*Mead and Fairfield*, 1975]; (2) OP, the Olson and Pfitzer model [*Olson and Pfitzer*, 1982]; (3) T87, the Tsyganenko model [*Tsyganenko*, 1987]; (4) T89, the Tsyganenko model [*Tsyganenko*, 1989]; (5) HV, the Hilmer and Voigt model [*Hilmer and Voigt*, 1995]; (6) T96, the Tsyganenko model [*Tsyganenko*, 1995, 1996]; (7) PM, the paraboloid model [*Alexeev et al.*, 1996]; (8) MO. the Maltsev and Ostapenko model [*Maltsev and Ostapenko*, 2001]; (9) T01, the Tsyganenko model [*Tsyganenko*, 2002]. A brief review of some magnetospheric magnetic field models is given below.

[79] The MF and MO models do not describe each of the large-scale magnetospheric current systems individually. Instead, the total current from all the external magnetic field sources (14 sources in the MO model) is calculated. In MF, T87, and T89 models, the *Kp* index characterizing the magnetic field disturbance intensity over a 3-hour interval is used, which restricts the possibility of detailed description of magnetic field variations during a magnetic storm.

[80] In the OP model, the ring currents are represented by elliptical wire loops with the innermost carrying eastward current and the rest of the loops carry westward current. The tail currents are also represented by elliptical loops. They consist of the dawn-to-dusk current in the plasma sheet with the closure currents around the lobes along the magnetopause. The shape of the magnetopause was found empirically, and it has the standoff distance (the distance from the Earth to the magnetopause along the Earth-Sun line) that scales according to magnetospheric activity. Scale factors were introduced for the ring current (according to the *Dst* index), and for magnetopause and the tail currents (according to the stand-off distance): magnetic field contributions of these current systems increase as the standoff distance decreases.

[81] The T87 model sums the contributions to the total magnetic field from three current systems. Both the ring and tail current contributions are given by analytic functions. The ring current is azimuthally symmetric and flows westward around the dipole. The tail current flows from dawn to dusk in the tail plasma sheet and in the two plane sheets parallel to the central one. Those simulate the return currents over the magnetopause. The magnetopause current contribution is represented by products of polynomials and decaying exponentials.

[82] The T89 model is comprised of six static models for different *Kp* levels. These static models are used sequentially to model storm periods as the *Kp* index changes. The model is an empirical fit to the data. It has no magnetopause surface. The ring and tail currents comprise axisymmetrical continuous current disks with only the westward directed current. This westward current does not have a low-altitude cutoff and it continues down through $L = 1$. The boundary between the ring and tail currents is absent as well. A pair of planar current sheets is used to simulate the return currents of the central tail current sheet.

[83] The HV magnetic field model is a dynamical model which uses four physical input parameters to adjust the magnetic fields of three current systems: ring (B_R), tail (B_T), and magnetopause (B_{CF}) currents. The magnetopause surface is presented by a semi-infinite cylinder with radius R and the dayside hemisphere with the same radius. The magnetopause standoff distance $R1$ is less than R so that the Earth lies sunward of the hemisphere-cylinder interface by a distance ($R - R1$). The B_{CF} field is determined from the boundary condition for the magnetopause magnetic field $\mathbf{n} \cdot (\mathbf{Bd} + \mathbf{B_{CF}}) = 0$. The tilt angle and the standoff distance are used to determine the magnetopause currents, which shield the dipole magnetic field. The ring and cross-tail currents remain unshielded. The ring current is azimuthally symmetric but there is an eastward current flowing within the westward current. The equatorward boundary of the diffuse aurora in the ionosphere maps magnetically to the magnetospheric equatorial plane at midnight (plasmapause). This distance is taken to be the inner (near-Earth) boundary of the current sheet. The tail current flows from dawn to dusk on a sheet which is comprised of 16 sets of filaments downtail. Each set has adjacent magnetic filaments of infinite extent in the $\pm y$ direction with varying current strength in order to model the decrease in current downtail. The near-Earth boundary of the tail plasma sheet in the midnight meridian is assumed at 10.5 R_E distance. The cross-tail current peaks near the inner edge and filament strength exponentially decreases moving tailward.

4.2.2. Recent Tsyganenko Models

[84] The T96 model is a substantially improved version of T87 and T89 models. The input parameters of the empirical-statistical model T96 are geomagnetic dipole tilt angle (Ψ), geomagnetic activity *Dst* index, solar wind dynamic pressure (*Psw*), IMF B_y and B_z components. The model is based on satellite measurements of magnetic fields at geocentric distances between 3 R_E and 70 R_E carried out by satellites IMP, HEOS, ISEE-1, and ISEE-2 within the time interval of 1966–1981.

[85] The magnetopause is introduced. It has the composite shape of a prolate semiellipsoid of revolution from the front side up to tailward distance of 60–70 R_E, smoothly continued in the far tail by a cylindrical surface. The existence of the magnetopause allows one to determine shielding magnetic fields for the Earth's dipole, the ring and cross-tail currents. A new model of the magnetic field of the cross-tail current was employed, including a gradual merging of the cross-tail and ring currents as well as a steep variation of the current density at the inner edge of the current sheet. The cross-tail current model allows the superposition of several independent modes with different rates of tailward decrease of the current density. The ring current B_R field was represented by a vector potential with a special choice of the weight coefficients and nonlinear parameters so that the radial profile of the current density is confined within a relatively narrow region inside 10–12 R_E and has a maximum at 6–8 R_E. The net contribution from external sources was taken as the sum of three terms (modules), namely B_T, B_{CF}, and B_R. The model fitting to the satellite data with different selections of variable free parameters is used.

[86] At present, various modifications of T89 and T96 models are available for representation of the large-scale magnetospheric configuration during storm periods. *Ganushkina et al.* [2002], using 15 May 1997 and 2 May 1998 storms as an example, obtained a more accurate and

Table 1. Input Parameters of the Magnetospheric Magnetic Field Models

Input Parameters	MF	OP	HV	T87	T89	MO	PM	T96	T01
x, y, z	*	*	*	*	*	*	*	*	*
Ψ	*	*	*	*	*	*	*	*	*
Kp	*			*	*	*			
Dst		*	*			*		*	*
Psw						*	*	*	*
G1									*
G2									*
B_y IMF							*	*	*
B_z IMF						*	*	*	*
DR							*		
R1		*	*				*		
R2							*		
R3[a]			*						
Φ							*		

[a]R3 is the geocentric distance to the plasmapause on the midnight meridian.

realistic representation of the magnetic field during magnetic storm times. The ring current of the T89 model was replaced by a new ring current representation. *Kubyshkina et al.* [1999] introduced a new approach to model the magnetotail observations during individual events. Such an event-oriented magnetospheric model uses, in addition to spacecraft magnetic measurements in the tail, other complementary information.

[87] The T01 model is a modification of a series of models and is now regarded as the new version of those already well-known and widely utilized models. This model is based on empirical modeling of the near-Earth magnetosphere at $x > -15\ R_E$. The database used to construct the T01 included a wide range of altitudes and latitudes covered by a number of satellites: Polar, Geotail, ISEE-2, AMPTE/CCE, AMPTE/IRM, CRRES, and DE-1. The model field is the sum of five physically different vector fields (B_{CF}, B_T, B_{RC}, B_{IMF}, B_{FAC}).

[88] Moreover, three of these external magnetic field contributions (due to cross-tail current, ring current, and field-aligned current) have been further split into sums of separate modules. For description of the magnetic field dawn-dusk asymmetry during disturbed times the ring current field B_{RC} is presented as a sum of two modules: the first module is the axially symmetric part of the ring current (SRC) and the second one represented the partial ring current (PRC). The amplitudes of SRC and PRC are represented as linear functions of the corrected index *Dst** and solar wind pressure *P*.

[89] In the T01 model the net external model field in its final form includes 24 coefficients and 18 nonlinear parameters, the values of which are to be determined from the data. The input parameters for the T01 model are the same as for T96 model, but two new parameters are added. Those are $G_1 = Vh(B_\perp)\sin^3(\Theta/2)$, where V is the solar wind velocity, Θ is the IMF clock angle, the function $h(B_\perp) = (B_\perp/40)^2/(1 + B_\perp/40)$, $B_\perp^2 = B_y^2 + B_z^2$, which controls the model magnetic field in the tail lobe, and $G_2 = \alpha(VB_s)$ which is proportional to the solar wind electric field, where V and B_s are the solar wind speed and the IMF southward component, respectively, averaged over the preceding 1-hour interval. The constant factor $\alpha = 0.005$.

[90] Actually, a much more detailed modular approach lies at the core of all recent Tsyganenko models, representing the total field as a sum of contributions from independent sources shielded within a realistic magnetopause. In particular, the magnetotail field in those models is fully confined inside the boundary, and the tail currents close over the entire magnetopause (including the dayside), in the same way as in the PM.

[91] The modular approach for magnetospheric magnetic field modeling was first suggested by *Alexeev and Shabansky* [1971], *Alexeev and Shabansky* [1972], and *Alexeev* [1978]. The magnetic field of the tail current system under the condition $B_{TN} = 0$ at the magnetopause was first formulated by *Alexeev et al.* [1975].This condition is equivalent to the tail current close over the entire magnetopause.

[92] To summarize the short overview of some magnetospheric magnetic field models, their input parameters are listed in Table 1. The description of these individual input parameters is given in the sections above.

4.2.3. Model Field Using the T96 and T01 Models Versus GOES 8 Geosynchronous Data

[93] Magnetospheric models T89, T96, and T01 are the most commonly used today for the modeling of global geomagnetic field. They are constructed as a best fit approximation of spacecraft measurements and reflect some important large-scale features of the magnetospheric configuration as well as trends in magnetospheric response to the varying solar wind parameters. This is a particularly good reason why the results of modeling magnetic fields in the magnetosphere for September 1998 by means of the PM model are compared below with the results of the T96 [*Tsyganenko*, 1995, 1996] and T01 [*Tsyganenko*, 2002] models.

[94] In Figures 11 and 12, comparisons of magnetic fields at geosynchronous orbit (solid line) with model calculations using T96 and T01 models (dotted lines in each figure) are presented. The correlation coefficients and dispersion between observed and modeled field components using T96 are displayed in Figure 11 for each magnetic field component and total field. They range from 0.71 to 0.99 and from 11.7 nT to 32.1 nT, respectively. Quite good agreement between the T96 model and observed field profiles appears to be even more curious in view of the fact that the ranges of solar wind plasma pressure and B_s values over which this model is valid are $Psw \leq 2.6$ nPa and $B_s < 10$ nT, respectively. These conditions are not fulfilled for the storm analyzed.

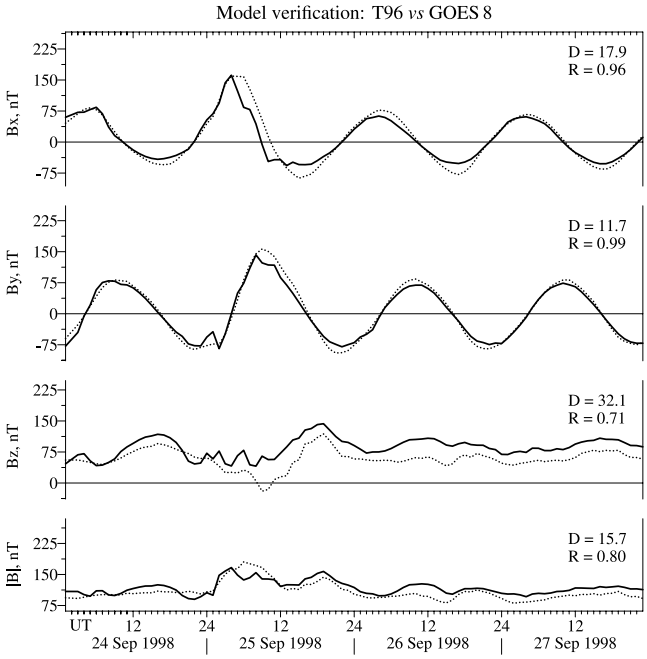

Figure 11. The Tsyganenko model T96. The comparison of measured (solid line) and modeled (dotted line) magnetic fields along the GOES-8 orbit: B_x GSM, B_y GSM, B_z GSM and total $|B|$ (from the top to the bottom).

[95] For the T01 model the correlation coefficients for individual field components vary within the range of 0.66–0.99, while dispersions range between 10.6 nT and 41.0 nT as seen in Figure 11. Worth noting is very good agreement between the model and observational values of the B_y component at geosynchronous orbit for both the T96 and T01 models.

4.3. Accuracy of Models

[96] The magnetic field calculated by means of the PM model shows good agreement with the observed profiles of geomagnetic field at geosynchronous orbit. Better agreement is seen in the B_z and $|B|$ profiles from the PM than is obtained using the T96 and T01 models.

[97] To summarize the results of modeling magnetic field variations, it can be emphasized that the models considered do adequately describe the magnetic field development within the interval of the magnetic storm at geosynchronous satellite distances. The existing models of the external magnetic field describe its variations at geosynchronous orbit well during storm time for both the total field and field components. The correlation coefficient obtained is >0.9; mean square deviation (dispersion) is ~20 nT. Such a correlation between modeled and observed magnetic field values at geosynchronous orbit is a validation of the success of these models in describing the large-scale configuration of the magnetosphere.

[98] The PM is universal since it is suitable either for quiet or disturbed conditions. The comparable accuracy of the PM and T96 (and/or T02) provides evidence for the validity of the PM in representing the magnetospheric configuration during severe magnetic storms.

[99] However, the lack of à partial ring current system (PRCS), which includes the current in the equatorial cross-section of the magnetosphere, the Region 2 FAC and the closure currents in the ionosphere, is the weakness of the PM. It cannot be ruled out that the agreement between the PM modeled and observed fields would be improved if the PRCS magnetic field were taken into account during the storm main phase. The consideration of this effect in the PM meets some difficulties since (1) nowadays, there were proposed the substantially different specification of the PRCS character including its magnetic field large-scale asymmetry (day-night and/or dawn-dusk), which is the basic PRCS feature [*Tsyganenko et al.*, 2003; *Pchelkin et al.*, 2004; *Le et al.*, 2004]; (2) the PRCS ranges among short-lasting (about an hour) current systems similarly to the substorm current wedge and transition current system [*Clauer et al.*, 2001]. The contribution of such current systems to disturbances at the low latitudes is sign-variable on local time. It means that their contribution to the *Dst* variation during the storm main phase is small in comparison with the magnetic field effect of the symmetric ring/magnetotail current. In fact, the contribution of short-lasting currents is possible only in the limited regions of the magnetosphere.

5. Discussion and Conclusion

[100] In this study the PM self-consistent version is used. Two input parameters, R1 (distance to the subsolar point on the magnetopause) and R2 (distance to the near-Earth current sheet boundary in the magnetotail) are determined by iterations. In each successive iteration, the magnetic field generated by model current systems defined within the preceding iteration is used to calculate new R1 and R2

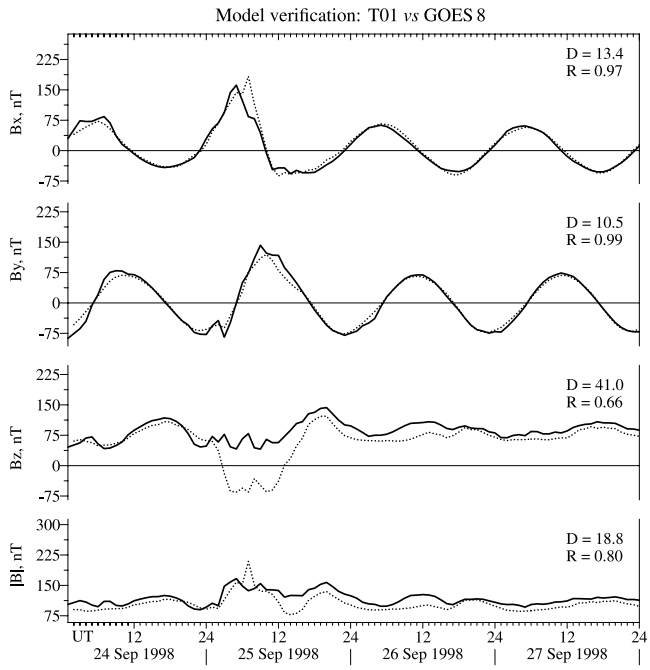

Figure 12. The Tsyganenko model T01. The comparison of measured (solid line) and modeled (dotted line) magnetic fields along the GOES-8 orbit: B_x GSM, B_y GSM, B_z GSM and total $|B|$ (from the top to the bottom).

values. Conversely, the intensity of the model current systems is defined successively using the obtained R1 and R2 values. So the self-consistency of the R1 and R2 values with the intensities of the current systems (dependent on R1 and R2) takes place due to iterations. Iterations continue until the difference between two consequent values R1 (N) − R1 (N − 1) is less than 0.1 R_E and between two consequent values R2 (N) − R2 (N − 1) is less than 0.2 R_E. The iteration procedures conserve for R1 the pressure balance at the subsolar point and for R2 the agreement between the model field line mapping distance to inner boundary of the tail current sheet and the parameter R2.

5.1. DCF Field

[101] It is worth noting that the well-known Chapman-Ferraro (CF) current, if considered realistically, is a net current system on the magnetopause resulting from several sources. The magnetopause current system is represented by current shielding the geomagnetic dipole, current shielding the ring current, current associated with the magnetotail current system, current associated with the high-latitude Region 1 FAC, and current shielding the remaining currents in the magnetosphere. Using the PM, *Alexeev and Feldstein* [2001] estimated the magnetic field of the CF current on the Earth's surface, DCF, as the field due to a net current system shielding both the geomagnetic dipole and ring current (DCF_{PM} estimate). On the other hand, *Kozyra et al.* [2002] used the relationship DCF = $bP^{1/2}$ to estimate this field in their model calculations (DCF_{SWP} estimate). The differences between these two estimates for the 24–27 September 1998 magnetic storm can be seen in Figure 8.

[102] The DCF_{SWP} estimate means that the solar wind dynamic pressure is balanced only by the magnetic pressure of the Earth's dipole magnetic field, i.e., the IMF dependence of the geocentric distance to the magnetopause subsolar point (R1) is omitted from consideration. Meanwhile, in the DCF_{PM} the radial distance at which pressure balance was achieved between the solar wind dynamic pressure and magnetospheric magnetic field pressure has moved to smaller radial distances (corresponding to larger values of the dipole field component) during IMF $B_z < 0$ for a fixed dynamic pressure $P(B_z < 0) = P(B_z > 0)$. Its decrease cannot be attributed to erosion due to magnetic reconnection (not explicitly represented in the PM), but rather must be due to other current systems responding to IMF $B_z < 0$ conditions. Those are magnetotail and Region 1 FAC currents. The magnetotail current flowing along the dayside magnetopause in the opposite direction to the CF currents weakens the magnetic field at the subsolar point if compared to the dipolar field at a given R1. In a similar way, the field from Region 1 FAC weakens the dipole magnetic field at the subsolar point. Hence during IMF $B_z < 0$ the magnetopause moves inward to find a pressure balance between the solar wind dynamic pressure and PM magnetic fields at smaller radial distances. The inward shifting of the dayside magnetopause during IMF $B_z < 0$ is also due to the enhanced magnetic flux in the tail lobes (enhancement of the magnetotail current) and the enhanced solar wind electric field (enhancement of the Region 1 FAC).

[103] During IMF $B_z < 0$ the real net CF current is located closer to the Earth and thus produces a larger DCF contribution to *Dst*. Consequently, $bP^{1/2}$ becomes a less accurate estimate of the CF current contribution to magnetic field intensity on the Earth's surface. Utilization of the $bP^{1/2}$ expression leads to an unchanged CF current contribution into the surface magnetic field, although it is apparent that the nearer to the Earth currents on the magnetopause are located the more intense their contribution to magnetic fields on the Earth's surface.

[104] The differences in R1 for the same solar wind dynamic pressure but for different magnetic field models (i.e., pressure balance in the PM and dipole approximation) are compared to R1 by *Shue et al.* [1997] (see Figure 2 in section 3.2). The different approaches to estimate R1 lead to differences in the DCF field variation.

5.2. DT/DR Relation

[105] The relative magnitudes of DT and DR magnetic field perturbations change as a magnetic storm progresses. Their ratio in the PM is DT/DR = 0.7–0.8 during the main phase, decreasing to DT/DR = 0.3–0.5 during the storm recovery phase. The variability of the relative contribution of disturbed magnetic fields associated with the magnetotail current and ring current during the storm time is due to the different decay timescales of the corresponding current systems. The decay rate of the DT current system [*Feldstein et al.*, 2000b] is ~5 hours, which is faster than that of the symmetric DR current system.

[106] The relationship between magnetic fields of ring and magnetotail currents during magnetic storms is now widely discussed by the scientific community. In the introduction different approaches to this issue were reviewed. A noteworthy result was reported by *Greenspan and Hamilton* [2000]. Observations of energetic ring current ions during 80 magnetic storms within the 1984–1989 time period near solar cycle maximum phase indicate a strong linear correlation between the global ring current energy content E_{RC} estimated using data from the nightside ion measurements and the *Dst* index. *Dst* is in good agreement with the prediction of the Dessler-Parker-Sckopke relationship. This implies that DR ~ *Dst*. The results reported by *Greenspan and Hamilton* [2000] do not preclude the possibility that the DT and DCF disturbance fields are approximately equal and opposite, on average canceling as in the PM. Unfortunately, they were unable to address the contribution of DCF to the *Dst* variations during the main phases of magnetic storms in the time interval studied most probably due to the lack of information on interplanetary plasma parameters.

[107] The PM analysis of the 24–27 September 1998 magnetic storm at the main phase maximum when *Dst* is −207 nT, gives DR = −167 nT (i.e., DR/*Dst* ~ 0.8). This ratio is consistent with the results of *Greenspan and Hamilton* [2000] obtained on the basis of observations from many magnetic storms. Values of DR and *Dst* are close to each other, but it does not imply a small value of the DT field. For the 24–27 September 1998 storm the maximum value of DT is −134 nT, when DT/DR = 0.8. It gives evidence of a comparable intensity of the magnetic field disturbances on the Earth's surface due to the current systems in the magnetospheric tail and the ring current.

[108] The evolution of existing ideas about both the role of DR and DT in generation of the *Dst* variation is quite evident in studies by Tsyganenko. According to his earlier results on the Earth surface, *Dst* = DR + DCF [*Tsyganenko*,

1995, 1996]. Later on *Tsyganenko et al.* [1999] stated: "The symmetric part of the Dst field is a sum of (1) the Chapman-Ferraro field from the magnetopause currents, proportional to $\sqrt{P}$ and (2) the field of B_E produced by other external sources, mostly by the ring current and to a lesser extent by the near-Earth part of the tail current sheet" [*Tsyganenko et al.*, 1999]. This means that there is some contribution of DT in *Dst* already, but that is substantially less than DR.

[109] The T01 model [*Tsyganenko*, 2002] takes into account possible earthward/tailward shift of the tail current. An additional degree of freedom was introduced, a variable shift ΔX of the inner boundary of the tail current sheet. It is assumed that magnitude of shift is proportional to the variation of the magnetospheric convection electric field and is described by the relation $\Delta X = \Delta X_0 + a\Delta X_1\ (V \times B_s)$, where V is the solar wind velocity, B_s is the IMF $B_z < 0$ component, the coefficients $a = 0.005$, $\Delta X_0 = 0.689$, $\Delta X_1 = -0.046$.

[110] Returning to consideration of the 24–27 September 1998 magnetic storm, during the main phase maximum (0800–1000 UT 25 September), $B_s \sim 13$ nT, $V \sim 800$ km/s, which gives a value of $\Delta X \sim -1.7$. In other words, for these conditions the parametrization in T01 gives a modeled tailward shift of the inner boundary of the magnetotail current sheet by 1.7 R_E. On 24 September at 0100–0200 UT, prior to the onset of the main phase of the magnetic storm, the current sheet inner boundary at MLT midnight was located at ~5.6 R_E. Adding the boundary shift calculated above to this prestorm value implies that T01 would model the inner edge of the magnetotail current sheet as moving outward to 7.3 R_E during the main phase at 0800–1000 UT 25 September. Naturally, such large tailward shift of the tail current leads to a decrease of the DT contribution to the *Dst* variation in comparison with the DR contribution. Apparently, this is one of the causes of DR prevailing over DT during the storm main phase using the T96 and T01 models.

[111] Summarizing his latest results on deriving an empirical model of the magnetospheric magnetic fields due to various sources, *Tsyganenko et al.* [2003] used as a basic approximation the T01 model. The treatment of the PRC was modified from that in T01 to introduce a dependence of the PRC strength on the solar wind density and to shorten the buildup and decay timescales for the PRC relative to *Dst* timescales.

[112] Several major magnetic storms were simulated with the result that DT reached values that were a significant fraction of DR in all cases. These latest results by *Tsyganenko et al.* [2003] on the relative magnitude of the contributions of DT and DR to the *Dst* disturbance of the geomagnetic field are consistent with significantly earlier statements by *Alexeev et al.* [1996] based on the PM model and by *Maltsev et al.* [1996]. Unfortunately, in the work of *Tsyganenko et al.* [2003] one cannot find any reference to these earlier results.

5.3. Current Sheet Inner Boundary

[113] The penetration of the inner boundary of the current sheet to the geocentric distance of (3.5–4.0) R_E in PM is regarded as a controversial assumption. *Turner et al.* [2000, 2002] supposed that the current sheet earthward boundary is located at $L \sim 6$ (or even more distant than the geosynchronous orbit) within the interval of the magnetic storm. The physical arguments for such a boundary location were not given. *Liemohn et al.* [2001a, 2001b] locate the current sheet boundary at $L > 6.6$, i.e., out of the region contained in their model.

[114] There is evidence to suggest that a magnetotail-like configuration exists at times to quite low L values. The beginnings of magnetic disturbances are accompanied with processes that produce plasma acceleration. Using the plasma observations on the CRRES satellite [*Friedel et al.*, 1996], the location of plasma sources in the equatorial plane of the magnetosphere during disturbed periods were determined along with location of the so-called "injection boundary." This boundary is the earthward boundary of the region where dipolarization of the magnetotail field is believed to simultaneously accelerate electrons and ions of all the energies at substorm onset. If the satellite location is within and/or quite near the injection boundary, the beginning of the disturbance is characterized by the absence of time dispersion in satellite observations of electrons over a wide range of energies. According to *Friedel et al.* [1996] the inner edge of the injection boundary as inferred from observations of electrons and protons with energies in the range $21 < E < 285$ keV (electrons) and 37 keV $< E <$ 3.2 MeV (protons) has been observed in the inner magnetosphere down to L values as low as $L \sim 4.3$ within ±5 hours of local geomagnetic time relative to the midnight. Hence the CRRES satellite observations and their analysis appear to be an independent confirmation of the approaches to the Earth of the plasma sheet inner (earthward) boundary up to $L \sim 4.3$ on the nightside during very strong magnetospheric disturbances.

[115] According to *Fairfield* [1980], the "hinging" distance that characterizes the location of the tail current sheet inner boundary at midnight shifts earthward during disturbed geomagnetic conditions. Indeed during a magnetic storm main phase the inner boundary of the plasma sheet at the midnight sector shifts earthward. When *Dst* equals ~ −120 nT, the inner boundary is located at $R \sim 3.5$ R_E [*Feldstein et al.*, 2000a]. At this geocentric distance according to AMPTE/CCE satellite measurements the pitch-angle distribution of auroral energy electrons changes from quasi-trapped to isotropic.

[116] According to *Alexeev et al.* [1996] and *Dremukhina et al.* [1999], the tail current sheet inner boundary is mapped to latitudes of the westward electrojet in the near midnight sector or to the b2e boundary of the electron precipitation. This MLT midnight boundary is located at mlat <60° at times during the storm main phase. If this boundary is mapped from the ionosphere to the magnetosphere along magnetic field lines, a geocentric distance of 3.5–4.0 R_E is obtained. This implies that the tail current sheet inner boundary is shifted during the storm main phase to these distances. This earthward shift of the tail current inner boundary leads naturally to a sharp distortion of the geomagnetic field in the inner magnetosphere. The assumed association between the westward auroral electrojet and magnetotail current provides further support for a location of the inner boundary of the tail current at low geocentric distances.

[117] This predicted distortion of the inner magnetosphere by the earthward shift of magnetotail currents is in agree-

ment with recent results using the T03 model [*Tsyganenko et al.*, 2003]. In T03 during the main phase of strong storms the inner magnetosphere becomes severely distorted. The quasi-dipolar approximation breaks down as close as $L \sim 3.5-4.0$, so that field lines with footpoints at $56-57^\circ$ mlat become essentially tail-like. Of course, some of this distortion is due to the partial/symmetric ring current itself and some portion is due to earthward penetration of strong magnetotail currents.

[118] The predictions [*Alexeev et al.*, 1996; *Dremukhina et al.*, 1999] of distortions of the inner magnetosphere by magnetotail currents differ from the newer T03 results only in the geomagnetic activity level that produces this low L value distortion. According to the PM, this already occurs during the main phase of moderate magnetic storms ($Dst \sim -150$ nT, $B_s \sim 15$ nT), while according to *Tsyganenko et al.* [2003] this occurs only during strong magnetic storms.

[119] Apparently, the T01 and T03 models use different relations for ΔX. For conditions at 2200 UT on 6 April 2000, the T01 model gives a tailward shift of the current sheet of -2.84. For such tailward shift of the current sheet boundary DR will substantially exceed DT on the Earth's surface. Unlike this model, PM predicts a significant contribution of DT to the *Dst* variation due to an earthward (rather than a tailward) shift of the tail current inner boundary during magnetic storm main phase. Unfortunately, data on the location of the inner boundary of the plasma sheet in the tail is not presented in the work of *Tsyganenko et al.* [2003].

6. Summary

[120] The PM magnetospheric model has incorporated a new iterative approach. The position of the subsolar magnetopause (R1) and the inner edge of the magnetotail current (R2) are iteratively determined. The magnetopause location is calculated using pressure balance between the external solar wind ram pressure and the magnetospheric magnetic field. The model takes into account the variation of the magnetic fields of self-consistent magnetospheric currents (ring current, magnetopause current, and the tail current) dependent on the IMF B_z. The output of this model gives different results for Chapman-Ferraro, magnetotail, and ring current fields from other magnetospheric models. These results have important consequences for our understanding of the internal magnetospheric structure and the magnetopause location. The model predictions are testable using spacecraft measurements. We plan on doing this for several magnetic storms in the near future.

[121] The major conclusions of this paper are as follows:

[122] 1. For large values of southward IMF component (B_s) during a magnetic storm main phase, the magnetic field on the Earth's surface calculated in PM (using the DCF field accepted) increases by several dozen nT over that calculated from simple pressure balance between the solar wind and Earth's dipole field. This increase is due to the weakening of the dayside magnetospheric fields by the field-aligned current and by tail current closure which shifts the magnetopause closer to the Earth in comparison with those values calculated without these additional current systems.

[123] 2. The ionospheric signature of the transition from adiabatic to nonadiabatic ring current energy ion motions in the magnetosphere (termed the b2i boundary) near midnight MLT shifts earthward from values of $(7-9)\ R_E$ during magneto-quiet intervals to values of $(3-4)\ R_E$ at a magnetic storm main phase maximum. This transition has been associated with a high degree of stretching in the equatorial magnetic field configuration. This is assumed to mark the earthward motion of the inner boundary of the magnetotail current system.

[124] 3. Fields of the magnetotail current system DT in PM contribute substantially to the *Dst* variation during the storm main phase. They are comparable to the DR contribution at this time but quickly decrease during a storm recovery phase (DT $\ll$ DR).

[125] 4. The decay parameter for the tail current system is substantially smaller (dissipation occurs quicker) than for the ring current.

[126] 5. Magnetic fluxes in the magnetotail lobes increase during the storm main phase to approximately twice their values at magneto-quiet intervals.

[127] 6. The calculated PM and observed GOES geosynchronous magnetic fields are in good agreement during the main phase of the 24–27 September 1998 magnetic storm event assuming an inward penetration of the magnetotail currents to R2–2 = 3–4 R_E. This supports the assumption that magnetotail currents penetrate earthward of the geosynchronous orbit during magnetic storms.

[128] 7. The PM model results indicate that during magnetic storms the geomagnetic field becomes essentially deformed on the nightside due to the displacement of the magnetotail current sheet to deep L shells ($L \sim 3.5-4.0$). At geosynchronous orbit, field lines are stretched in the antisunward direction. Models that describe the particle motion during the magnetic storm must take into account this stretched magnetic field geometry on the nightside.

Appendix A

[129] The purpose of this appendix is to further explore the ability of the PM model to reproduce realistic magnetic field configurations using additional data sets during the September 1998 magnetic storm (subsection A1.1) and similar model/data comparisons during a storm in May 1998 (section A2). In addition, a comparison is made between PM isocontours of azimuthal currents and those from the *Tsyganenko et al.* [2003] model and underlying database under similar Dst conditions (subsection A1.2).

A1. Modeling of the 24–26 September 1998 Magnetic Storm

A1.1 Comparison of Measured and Modeled Magnetic Fields Along the GOES-10 Orbit

[130] The magnetic field at geosynchronous orbit, modeled by the PM for 3 days of the September 1998 storm, is compared to observations by GOES-10. The GOES-10 satellite was in the evening/premidnight sector during the development of the storm main phase. At the main phase maximum GOES-10 entered the near-midnight sector of the magnetotail current sheet. The solar-magnetospheric (GSM) B_x, B_y, B_z components from PM (dashed line) are compared with the GOES measurements (solid line) in Figure A1. Local geomagnetic midnight corresponds to 0900 UT in the figure.

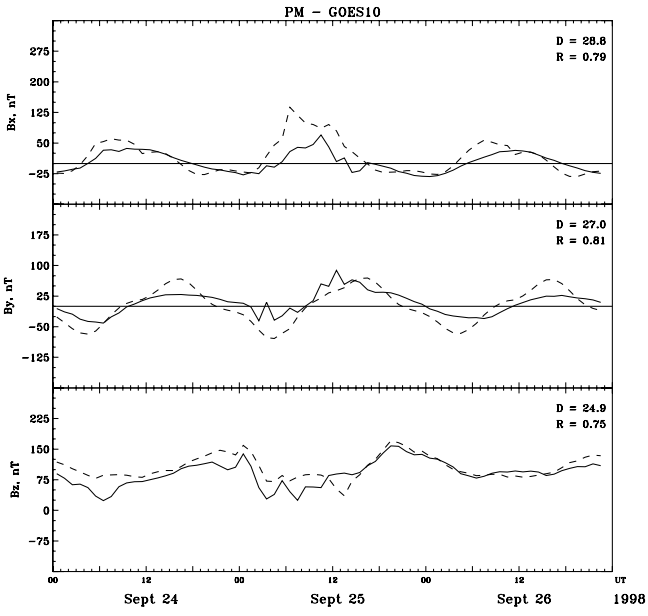

Figure A1. PM modeling of the 24–27 September 1998 magnetic storm. The comparison of measured (solid line) and modeled (dashed line) magnetic fields along the GOES-10 orbit: B_x GSM, B_y GSM, B_z GSM (from the top to the bottom).

[131] As seen, the model reproduces the measured field quite well at geosynchronous orbit. The corresponding correlation coefficients between modeled and observed values for each component range between 0.75 and 0.81. In other words, the PM reproduces the space-time variation of the field quite adequately for this storm. The mean quadratic deviations range between 24.9 nT and 28.8 nT compared to variations in amplitude of ~150 nT in this region. The differences between the measured and modeled geosynchronous field values provide an estimate of the magnitude of possible errors introduced by the lack of a partial ring current and substorm current wedge in the present version of the PM.

[132] In addition, when the dipole tilt angle is taken into account improperly, the agreement between observations and model results worsens. Even around equinoctial intervals as in the September 1998 storm, it is clear that the proper usage of Ψ, especially of the hinging effect, is an important point in producing a realistic representation of the magnetic field.

A1.2. Isocontours of the Azimuthal Currents Flowing in the Magnetospheric Equatorial Plane During Magnetic Storms

[133] As a further test of the PM model, isocontours of the azimuthal westward current according to *Pchelkin et al.* [2004] and those based on the PM were compared. The azimuthal westward current (in kA/R_E) flowing in the layer $|z| < 3\ R_E$ was calculated *Pchelkin et al.* [2004] using two different methods: azimuthal currents (not shown for the sake of brevity) were extracted from the *Tsyganenko et al.* [2003] model (first method) or were obtained directly from the database of *Tsyganenko et al.* [2003] by differentiating a smoothed magnetic field during conditions associated with $Dst = -140$ nT (second method). If those are compared with isocontours of the azimuthal current flowing in the tail current sheet given by the PM during September 1998 for comparable *Dst* values (Figure A2), both similarities and differences can be seen between the models. All the isocontours do clearly show that the westward current in the inner magnetosphere is highly asymmetrical for the dayside and nightside magnetosphere. The nightside current is stronger than the dayside one. The maximum of the linear current density of 1–2 MA/R_E occurs centered near midnight. During the main phase total currents at the midnight meridian between $-3\ R_E$ and $-10\ R_E$ in the PM reach intensities from 6 MA to 10 MA. Corresponding total current in the *Tsyganenko et al.* [2003] model between $-2\ R_E$ and $-9\ R_E$ is ~ 9.6 MA and from the database of

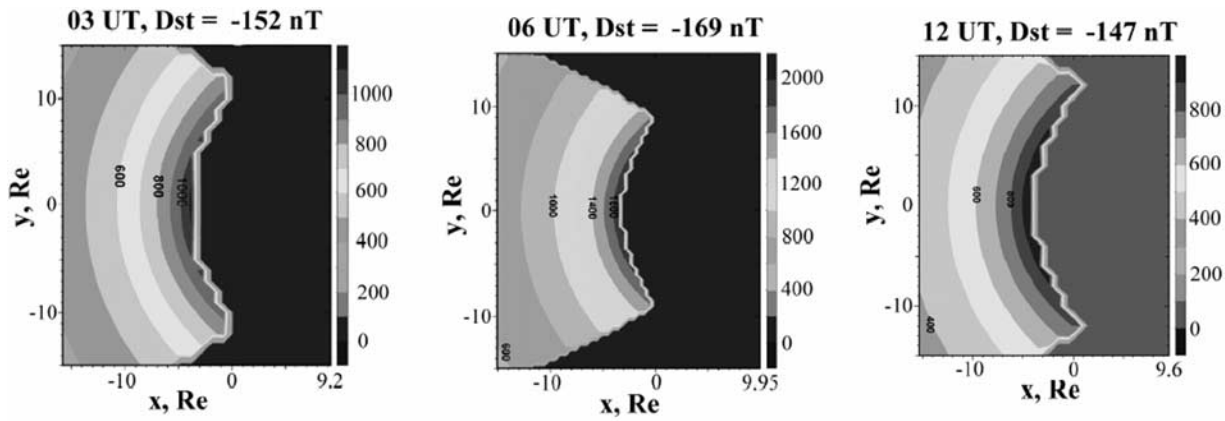

Figure A2. Isocontours of the azimuthal current flowing in the tail current sheet calculated by the PM for comparable [*Pchelkin et al.*, 2004] *Dst* conditions: just before the main phase, namely at 03 UT, when $Dst = -152$ nT, ÀL = −750 nT, R1 = 8.2 R_E, R2 = 3.8 R_E, $\Phi = 0.91 \times 10^9$ Wb and the linear current density maximum at the inner boundary is $j_{max} = 1122$ kA/R_E (left); during the main phase, namely at 0600 UT, when $Dst = -169$ nT, ÀL = −1374 nT, R1 = 6.3 R_E, R2 = 3.05 R_E, $\Phi = 1.0 \times 10^9$ Wb, j_{max} = 2040 kA/R_E (middle); during the recovery phase, namely at 1200 UT, when $Dst = -147$ nT, AL = −1139 nT, R1 = 9.3 R_E, R2 = 3.4 R_E, $\Phi = 0.97 \times 10^9$ Wb, $j_{max} = 1037$ kA/R_E (right).

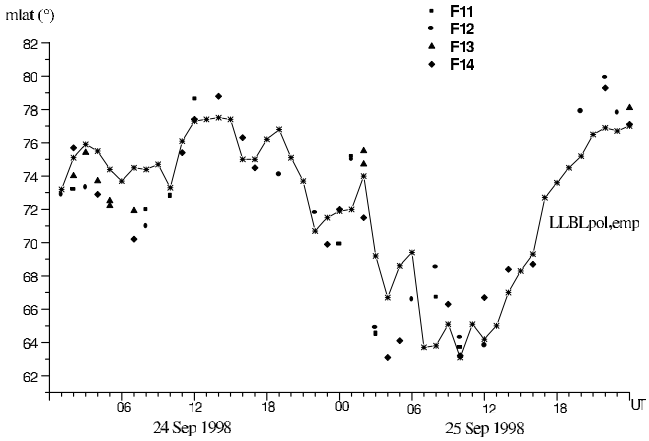

Figure A3. Variations of the LLBLpol boundary location (mlat hourly values) for successive UT hours on 24–25 September 1998: empirical LLBLpol,emp values (line with asterisk) and observed LLBLpol,dmsp data (DMSP F11, F12, F13, and F14 satellites as indicated in figure).

Tsyganenko et al. [2003] is ~11.5 MA. In the PM isocontours, the ring current contribution was not taken into account. The *Tsyganenko et al.* [2003] isocontours, however, include both the tail and ring current contributions to the total current across the Earth-Sun line located between $-2\ R_E$ and $-9\ R_E$. If the inner boundary between tail and ring currents is located at $-5\ R_E$ in the T03 model [*Tsyganenko et al.*, 2003] then the total tail current between this boundary and $-10\ R_E$ is equal to 7.7 MA. If tail/ring current boundary in the *Tsyganenko et al.* [2003] database is located at $-6\ R_E$ then the total tail current is 7.0 MA. Both estimates are close to the PM total value of the tail current: (6–10) MA.

[134] Differences in the model results are associated with the assumed distances to the region of the current maximum value. For the PM the westward current maximum is located at the inner boundary of the current sheet at about 3–4 R_E tailward during the main phase. In the T03 model this maximum is located at $-5\ R_E$, while for the database of *Tsyganenko et al.* [2003] it is at 6–8 R_E tailward. Moreover, in the framework of the PM the maximum of the westward current is not fixed and during the storm phase shifts earthward to noted 3–4 R_E from the 6–7 R_E distance which corresponds to relatively magneto-quiet intervals. According to *Pchelkin et al.* [2004], using the *Tsyganenko et al.* [2003] model and underlying database, the location of the current maximum does not depend on geomagnetic activity. This assumption appears to be based on very few data points inside geosynchronous orbit in the *Tsyganenko et al.* [2003] database. Additional magnetic field measurements in the region of 3–5 R_E are necessary to better define the location of maximum current and its variation during changing geomagnetic activity.

[135] Distributions of current intensities calculated using the PM and T03 models, as well as results obtained by *Pchelkin et al.* [2004] from the database by *Tsyganenko et al.* [2003] do unanimously indicate the essential contribution of tail currents to magnetic field depression and distortions in the inner magnetosphere during magnetic storm intervals. *Skoug et al.* [2003] even suggest from ENA observations a dominant tail current contribution in the inner magnetosphere during the main phase of the 31 March 2001 intense magnetic storm.

A1.3. Comparison of the Plasma Precipitation Boundaries: Calculated (Empirical) and Observed (DMSP) Data

[136] The PM input parameters were calculated using (4), (6), and (7). The empirical values for plasma boundary locations and corresponding observed data (a number of DMSP passages) for the September 1998 storm are directly compared below. DMSP passages on the dayside in the northern hemisphere took place quite frequently during 24–25 September 1998 allowing a comparison between calculated (using (7)) and observed plasma boundaries during different phases of the magnetic storm. In Figure A3 the variations in the LLBLpol mlat (line with asterisk for empirical values), as in Figure 5 (subsection 3.2.1.), can be seen for successive UT hours on 24–25 September 1998. The boundary locations from different satellites passages are also indicated. For given UT all the values available for all DMSP passages are shown. It is worth noting that boundary latitudes at the APL website in general correspond to the plasma structure boundaries as seen in original spectrograms. The agreement is apparent for both the mlat values and time-dependence pattern of the boundary location during the magnetic storm: (1) Before the storm the LLBLpol boundary is at ~74–76° mlat, i.e., at quite high latitudes. (2) Magnetic disturbances just before the storm main phase and especially during the main phase are accompanied by a remarkable equatorward shift of the boundary. (3) At the main phase maximum the LLBLpol boundary is at ~63–65° mlat. (4) During the recovery phase the boundary quickly returns to ~78° mlat.

[137] The LLBLpol shift during the main phase of the 24–25 September magnetic storm to as low mlat as ~64° is also characteristic for other intense storms. According to the

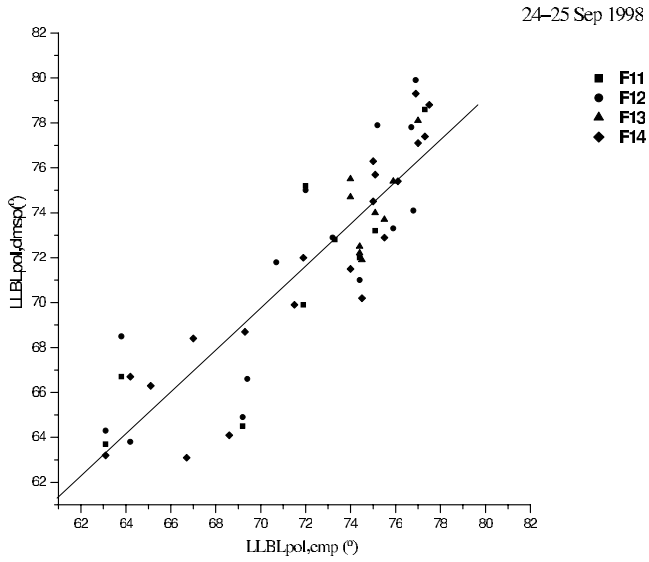

Figure A4. The relationship between the empirical LLBLpol,emp (x axis) and observed LLBLpol,dmsp (y axis) data for the 24–25 September 1998 interval. The corresponding regression line is also shown.

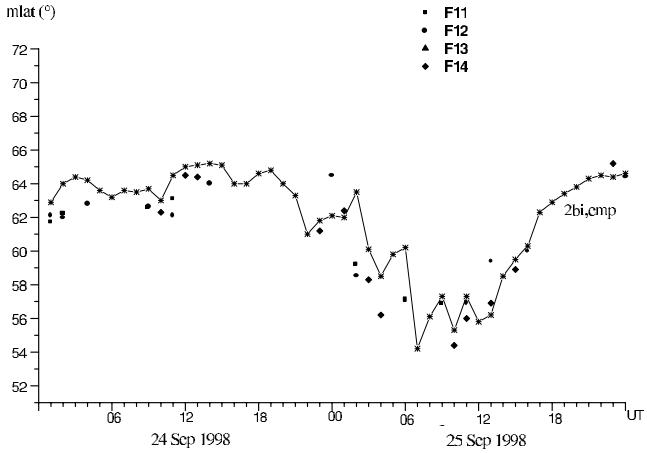

Figure A5. Same as in Figure A3, but for the empirical 2bi,emp and observed 2bi,dmsp data.

DMSP measurements a similar LLBLpol shift occurred during the 4 May 1998 storm main phase (day hours): (1) At 0400 UT the LLBLpol shifted to ~62° and 63.1° mlat according to DMSP F11 and DMSP F14 data; at 0500 UT the LLBLpol was at 62.7 mlat according to DMSP F12 data. (2) According to the parametric relationship (7), the LLBLpol location is predicted to be 64.5° (at 0400 UT) and 62.4° mlat (at 0500 UT), which is in quite good agreement with satellite measurements.

[138] As reported by *Meng* [1983, 1984], according to DMSP data the cusp equatorward boundary on the dayside shifted to mlat ~ 64° during magnetic storms considered. The equatorward shift to such a latitude is also confirmed by ground-based measurements. In fact, according to the rocket, balloon, and ionosonde measurements the dayside polar cusp was observed to shift to mlat values <60° during the magnetic storm on 19 December 1980 [*Bering et al.*, 1991].

[139] The relationship between the calculated and observed LLBLpol mlat values on the dayside during the 24–25 September interval can be seen in Figure A4. The calculated LLBL values (equation (7)) for successive UT hours, LLBLpol,emp (x axis), are plotted against the LLBLpol,dmsp mlat values (y axis). The relationship between boundary locations is described by the equation of linear regression LLBLpol,dmsp = 0.94 × LLBLpol, emp + 4.31°. The correlation coefficient is 0.88 and standard deviation is 2.28°.

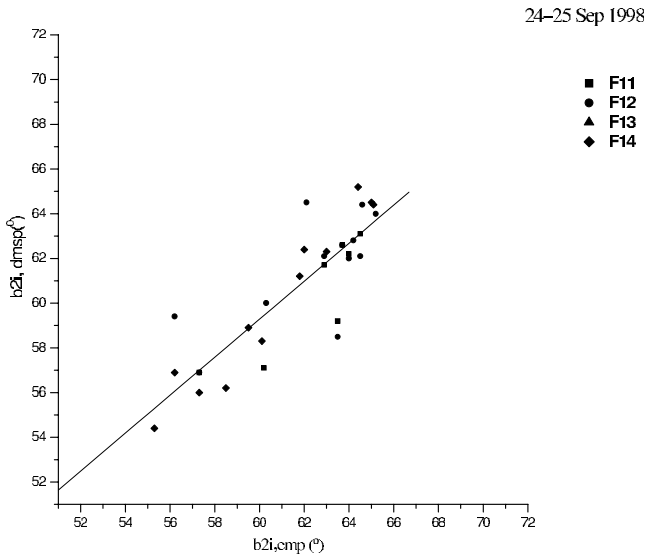

Figure A6. Same as in Figure A4, but for the empirical 2bi,emp and observed 2bi,dmsp data.

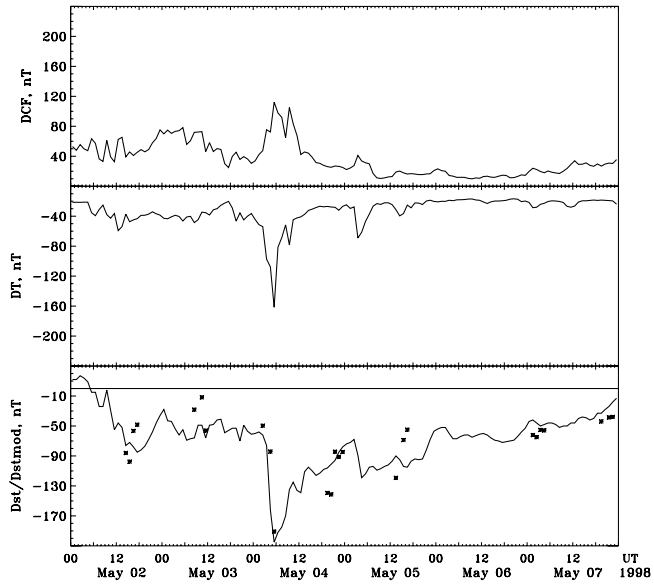

Figure A7. Variations of the magnetic fields on the Earth's surface including the fields of the induction currents in the solid Earth during the 2–7 May 1998 storm as observed and as calculated by the PM. Shown (from the top to the bottom) are the magnetic field disturbances due to: the magnetopause current (DCF); the tail current (DT); *Dst* based on observations (solid line) and Dst_{mod} = DCF + DT + DR (crosses).

[140] The other PM input parameters are defined by boundary locations on the nightside. Unfortunately, such measurements for the 24–25 September magnetic storm are not available in the northern hemisphere. This lack of data on plasma precipitation boundaries for individual storms was one of the reasons to develop empirical relationships (equations (4)–(7)) for these boundary locations. Meanwhile, there are a limited number of DMSP orbits crossing the b2i boundary in the southern hemisphere. All the b2i values are shown in Figure A5, where the southern latitude is changed the northern one assuming magnetic conjugacy in the boundary locations for the two hemispheres. Magnetic conjugacy is a reasonable assumption for b2i due to its location deep in the inner magnetosphere. As seen in Figure A5, the calculated boundary (equation (4)), b2i,emp, and boundary determined from DMSP data near midnight, b2i,dmsp, are in a good agreement. The location of b2i,emp moves from 62–64° mlat before the storm to 54–56° mlat during the storm main phase and then returns to 64° mlat during the recovery phase. The relationship between calculated and observed b2i values on the nightside for the 24–25 September 1998 magnetic storm can be seen in Figure A6, where all available DMSP measurements are

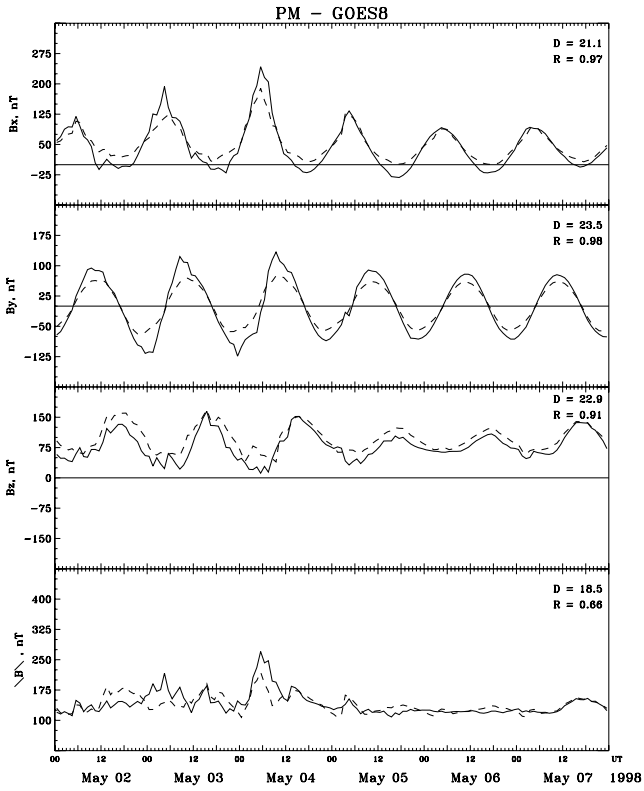

Figure A8. PM model results from the 2–7 May 1998 magnetic storm interval. Shown are the measured (solid line) and modeled (dashed line) magnetic fields along the GOES-8 orbit, including from the top to the bottom: B_x GSM, B_y GSM, B_z GSM and total $|B|$.

included. The b2i,emp (equation (4)) values on the x axis are plotted against b2i,dmsp values for corresponding hours along y axis. This relationship is described by the equation of linear regression b2i,dmsp = 0.85 × b2i,emp + 8.32° with the correlation coefficient of 0.86 and standard deviation of 1.56°.

[141] The shape of the polar cap is essential to calculate the magnetic flux in the magnetotail. Equations (2) and (3) approximate the polar cap boundary as a circle. The statistical significance of this approximation was analyzed by *Starkov et al.* [2003]. As a matter of fact, the polar cap boundary is oval-like with major axis in the direction noon-midnight (quiet conditions) or dawn-dusk (disturbed conditions). If the oval major axes are L_1 (noon-midnight) and L_2 (dawn-dusk), then the L_1/L_2 ratio ranges between 1.15 (quiet conditions) and 0.85 (disturbed conditions). Such changes in the polar cap configuration justify the approximate circular shape of the polar cap assumed in the calculation of magnetotail flux.

A2. Modeling of the 2–7 May 1998 Magnetic Storm

A2.1. Variations of the Magnetic Fields on the Earth's Surface

[142] To further explore the ability of the PM, driven by observed magnetospheric boundary locations, to reproduce magnetic field observations, model/data comparisons were performed for an interval of geomagnetic activity during 2–7 May 1998 triggered by high speed solar wind streams. Two separate interplanetary high-speed streams were observed. The first began with a shock at ~2115 UT 1 May and ended at ~1600 UT 3 May. The second stream started at ~0230 UT 4 May again with a shock and ended on 6 May. One small and one large magnetic storm resulted. The peak *Dst* values for the storms were −85 nT on 2 May 1700 UT and −205 nT on 4 May 0500 UT.

[143] The DT/DCF ratios within the 3-hour interval (UT) centered with respect to the *Dst* variation maximum are 0.94 and 1.24 for the first and second storm, while DT/DR are 0.5 and 0.71, respectively.

[144] In Figure A7 the DCF, DT, and *Dst* magnetic field variations for the 2–7 May interval are shown. To define DR in model calculations ion data from CAMMICE instrument on board the Polar spacecraft were used. Ions in the energy range from 6 to 400 keV e^{-1} [*Turner et al.*, 2001] were measured. Energy density is calculated as a function of L for each pass of the satellite and integrated over the pitch angle distribution. The energy content is the product of the energy density and the volume contained in each L shell. The ring current magnetic field intensity is defined under the standard assumption that *Dst*, once corrected for the influence of other current systems, is the reliable measure of the energy content in the ring current. The relationship between DR and the energy of the ring current particles is derived by Dessler-Parker-Sckopke relation.

[145] Data reported by *Turner et al.* [2001] make it possible to obtain DR values on the Earth's surface for each Polar pass. The duration of the $2 < L < 6$ shell intersection was ~1.5–2 hours and took place on day (1000 MLT) and night (2200 MLT) time intervals. Because of asymmetry in the azimuthal distribution of the ion density in the ring current an additional correction was introduced by *Turner et al.* [2001].

[146] The *Dst* variation based on observational data is shown in Figure A7 (solid line). For comparison the results of the PM calculations using the standard relationship Dst_{mod} = DCF + DT + DR are also shown (crosses). The DCF and DT variations were calculated on the basis of the PM expressions. DR was determined according to *Turner et al.* [2001]. Since the satellite traversed the ring current region in ~1.5–2 hours, hourly values of DCF and DT were considered. However, the same DR values were used.

[147] The Dst_{mod} profile follows that of *Dst* during the entire disturbed period, including its depression during the storms on 2 May and 4 May. The Dst_{mod} and *Dst* intensities differ only slightly, leading to the following conclusions: (1) *Dst* estimated by the PM are consistent with observations of magnetic variations (*Dst*) on the Earth's surface during magnetic storms. (2) The PM can be used for modeling without any free parameters, i.e., all the model input parameters are defined from independent observations; namely, the ring current magnetic field is defined from satellite observations of total energy of ring current ions.

A2.2. Comparison of Measured and Modeled Magnetic Fields Along the GOES-8 Orbit

[148] The variations of the magnetic field GSM components measured by geosynchronous GOES-8 satellite (solid line) and those calculated by means of the PM (dashed line) for the 2–7 May 1998 interval are shown in Figure A8.

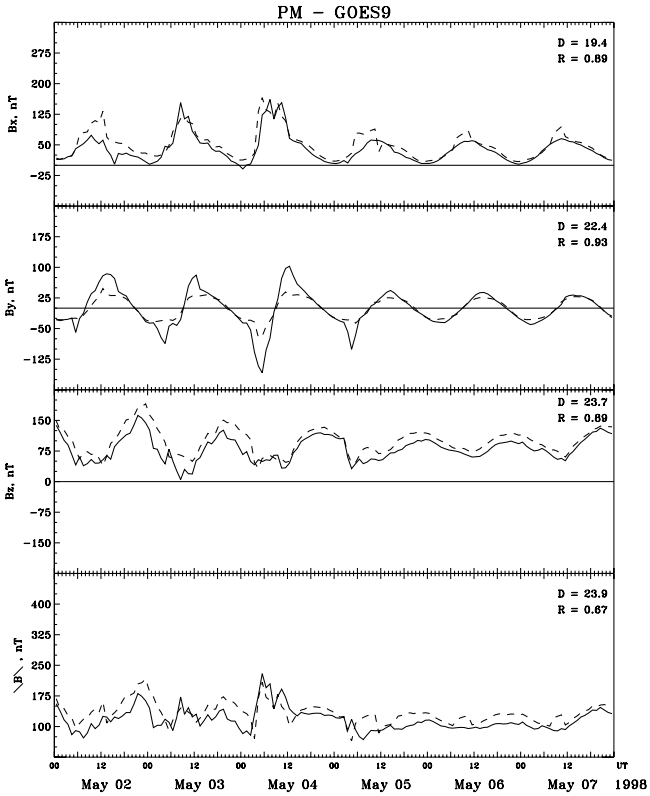

Figure A9. Same as in Figure A8, but along the GOES-9 orbit.

[149] Midnight MLT corresponds to 0500 UT in the figure. The high correlation coefficients between modeled and observed values for each component (>0.9) and relatively low dispersion (~10% of the variation amplitude) give evidence that the model reproduces the measured field quite well. The event occurred during summer when the absolute value of the dipole tilt angle exceeds ~25°. The reasonable fit of observed and modeled field components implies that the planar approximation for the tail current is also valid for this event. The consistency between modeled and observed fields was obtained by consideration the hinging effect only. If a current sheet deformation (the warping effect) is also taken into account, small corrections to the magnetic field are obtained very near the current sheet and those are local in nature.

A2.3. Comparison of Measured and Modeled Magnetic Fields Along the GOES-9 Orbit

[150] The variations of the magnetic field GSM components measured by geosynchronous GOES-9 satellite (solid line) and those calculated by means of the PM (dashed line) for the 2–7 May 1998 interval are shown in Figure A9. Midnight MLT corresponds to 1000 UT in the figure. At the maximum of the storm main phase, GOES-9 was in the evening sector. The high correlation coefficients between model and observational values for each component (>0.9) and relatively low dispersion (~8% of the variation amplitude) give evidence that the PM in its present form reasonably approximates the measured magnetic field at geosynchronous altitudes.

[151] **Acknowledgments.** We would like to thank WDC C2 for Geomagnetism, Kyoto for the provisional *AL* and *Dst* indices data, the Principal Investigators and realization teams of space experiments, who provided the data on solar wind (K. Oglivie, NASA/GSFC), IMF (R. Lepping, NASA/GSFC), GOES 8 magnetic field data (H. Singer, NOAA/SEC, Boulder), boundaries of auroral particle precipitations on DMSP (P. Newell, APL JHU, Laurel), D. Hardy (AFRL, Hanscom AFB) who designed and built the DMSP SSJ/4 particle detectors employed in this study. We are thankful to Y. P. Maltsev, V.V. Kalegaev, and S.Y. Bobrovnikov for valuable discussions. One of the authors (YIF) is grateful to B. Hultqvist and A. Nishida for helpful comments and constructive discussions. Portions of this research were performed at the Jet Propulsion Laboratory, California Institute of Technology under contract with NASA and under the following grants: grants 2/2009 and 2/5121 from Slovak Academy of Sciences; INTAS grant 03-051-5359 and RFFI grant 05-05-65196 (IZMIRAN); Conselho Nacional de Desenvolvimento Cientifico e Technologico, CNPq of Brasil; RFBR grant 00-15-96623 to INP-MU; one of the authors (J. Kozyra) would like to express appreciation for funding under NASA grants NAG5-10297 and NAG-10850 and NSF grant ATM-0090165. The authors are grateful to the staff of the International Space Science Institute, Bern, Switzerland for their hospitality and support of our project.

[152] Arthur Richmond thanks Y. P. Maltsev and two other reviewers for their assistance in evaluating this paper.

References

Akasofu, S.-I. (2002), *Exploring the Secrets of the Aurora*, 235 pp., Springer, New York.

Alexeev, I. I. (1978), Regular magnetic field in the Earth's magnetosphere (in Russian), *Geomagn. Aeron.*, *18*, 656–665.

Alexeev, I. I., and Y. I. Feldstein (2001), Modeling of geomagnetic field during magnetic storms and comparison with observations, *J. Atmos. Sol. Terr. Phys.*, *63*, 431–440.

Alexeev, I. I., and V. P. Shabansky (1971), Model of magnetospheric magnetic field (in Russian), *Geomagn. Aeron.*, *11*, 571–579.

Alexeev, I. I., and V. P. Shabansky (1972), A model of a magnetic field in the geomagnetopshere, *Planet. Space Sci.*, *20*, 117–133.

Alexeev, I. I., A. A. Kirilov, and T. A. Chujkova (1975), Geomagnetic tail current system (in Russian), *Geomagn. Aeron.*, *15*, 508–514.

Alexeev, I. I., E. S. Belenkaya, V. V. Kalegaev, Y. I. Feldstein, and A. Grafe (1996), Magnetic storms and magnetotail currents, *J. Geophys. Res.*, *101*, 7737–7747.

Alexeev, I. I., E. S. Belenkaya, and C. R. Clauer (2000), A model of Region 1 field-aligned currents dependent on ionospheric conductivity and solar wind parameters, *J. Geophys. Res.*, *105*, 21,119–21,227.

Alexeev, I. I., E. S. Belenkaya, S. Y. Bobrovnikov, and V. V. Kalegaev (2003), Modeling of the electromagnetic field in the interplanetary space and in the Earth's magnetosphere, *Space Sci. Rev.*, *107*(1–2), 7–26.

Angelopoulos, V., M. Temerin, J. Roth, F. S. Mozer, D. Weimer, and M. R. Hairtson (2002), Testing global storm-time electric field models using particle spectra on multiple spacecraft, *J. Geophys. Res.*, *107*(A8), 1194, doi:10.1029/2001JA900174.

Baker, D. N., N. E. Turner, and T. I. Pulkkinen (2001), Energy transport and dissipation in the magnetosphere during geomagnetic storms, *J. Atmos. Sol. Terr. Phys.*, *63*, 421–429.

Baker, J. B., C. R. Clauer, A. J. Ridley, V. O. Papitashvili, M. J. Brittnacher, and P. T. Newell (2000), The nightside poleward boundary of the auroral oval as seen by DMSP and Ultraviolet Imager, *J. Geophys. Res.*, *105*, 21,267–21,280.

Belova, E. G., and Y. P. Maltsev (1994), Supplementary sources of geomagnetic depressions during the geomagnetic storm of 8–9 February 1986, *J. Atmos. Sol. Terr. Phys.*, *56*, 1011–1015.

Bering, E. A., J. R. Benbrook, R. Haacke, J. R. Dudeney, L. J. Lanzerotti, C. G. Maclennan, and T. J. Rosenberg (1991), The intense magnetic storm on December 19, 1980: Observations at $L = 4$, *J. Geophys. Res.*, *96*, 5597–5617.

Borovsky, J. E., M. F. Thomsen, D. J. McComas, T. E. Cayton, and D. J. Knipp (1998), Magnetospheric dynamics and mass flow during the November 1993 storm, *J. Geophys. Res.*, *103*, 26,373–26,394.

Brittnacher, M., M. Fillingim, G. Parks, G. Germany, and J. Spann (1999), Polar cap area and boundary motion during substorms, *J. Geophys. Res.*, *104*, 12,251–12,262.

Burton, R. K., R. L. McPherron, and C. T. Russell (1975), An empirical relationship between interplanetary conditions and *Dst*, *J. Geophys. Res.*, *80*, 4204–4214.

Clauer, C. R., I. I. Alexeev, E. S. Belenkaya, and J. B. Baker (2001), Special features of the September 24–27, 1998 storm during high solar wind dynamic pressure and northward interplanetary magnetic field, *J. Geophys. Res.*, *106*, 25,695–25,711.

Craven, J. D., and L. A. Frank (1985), The temporal evolution of a small auroral substorm as viewed from high altitudes with Dynamics Explorer 1, *Geophys. Res. Lett.*, *12*, 465–468.

Daglis, I. A., J. U. Kozyra, Y. Kamide, D. Vassiliadis, A. S. Sharma, M. W. Liemohn, W. Gonzalez, B. T. Tsurutani, and G. Lu (2003), Intense space storms: Critical issues and open disputes, *J. Geophys. Res.*, *108*(A5), 1208, doi:10.1029/2002JA009722.

Dremukhina, L. A., Y. I. Feldstein, I. I. Alexeev, V. V. Kalagaev, and M. E. Greenspan (1999), Structure of the magnetospheric field during magnetic storms, *J. Geophys. Res.*, *104*, 28,351–28,360.

Fairfield, D. H. (1980), A statistical determination of the shape and position of the geomagnetic neutral sheet, *J. Geophys. Res.*, *85*, 775–780.

Fairfield, D. H., and A. F. Vinas (1984), The inner edge of the plasma sheet and the diffuse aurora, *J. Geophys. Res.*, *89*, 841–854.

Feldstein, Y. I., and Y. I. Galperin (1985), The auroral luminosity structure in the high-latitude upper atmosphere: Its dynamics and relationship to the large-scale structure of the Earth's magnetosphere, *Rev. Geophys.*, *23*, 217–275.

Feldstein, Y. I., and Y. I. Galperin (1993), An alternative interpretation of auroral precipitation and luminosity observations from the DE, DMSP, AUREOL, and Viking satellites in terms of their mapping to the nightside magnetosphire, *J. Atmos. Sol. Terr. Phys.*, *55*, 105–121.

Feldstein, Y. I., and Y. I. Galperin (1996), Structure of the auroral precipitations in the nightside sector of the magnetosphere (in Russian), *Cosmic Res.*, *34*(3), 209–227.

Feldstein, Y. I., L. A. Dremukhina, and A. T. Y. Lui (2000a), Near-Earth (inner) boundary of the tail plasma sheet during magnetic storm (in Russian), *Geomagn. Aeron.*, *40*(6), 122–123.

Feldstein, Y. I., L. A. Dremukhina, U. Mall, and J. Woch (2000b), On the two-phase decay of the *Dst* variation, *Geophys. Res. Lett.*, *27*, 2813–2816.

Frank, L. A., J. B. Sigwarth, and W. R. Paterson (1998), High-resolution global images of Earth's auroras during substorms, in *Substorms-4*, edited by S. Kokubun and Y. Kamide, pp. 3–8, Springer, New York.

Friedel, R. H. W., A. Korth, and G. Kremser (1996), Substorm onsets observed by CRRES: Determination of energetic particle source region, *J. Geophys. Res.*, *101*, 13,137–13,154.

Galperin, Y. I., J. Crasnier, Y. V. Lissakov, L. M. Nikolaenko, V. M. Sinitsin, J. A. Sauvaud, and V. L. Khalipov (1977), Diffuse auroral zone: 1. A model of the equatorial boundary of the auroral electron diffuse precipitation zone in the evening and near-midnight sectors, *Cosmic Res.*, *15*, 421–434.

Galperin, Y. I., V. S. Soloviev, K. Torkar, J. C. Foster, and M. V. Veselov (1997), Predicting plasmaspheric radial density profiles, *J. Geophys. Res.*, *102*, 2079–2091.

Ganushkina, N. Y., T. I. Pulkkinen, M. V. Kubyshkina, H. J. Singer, and C. T. Russell (2002), Modeling the ring current magnetic field during storms, *J. Geophys. Res.*, *107*(A7), 1092, doi:10.1029/2001JA900101.

Gonzalez, W. D., J. A. Joselyn, Y. Kamide, H. W. Kroehl, G. Rostoker, B. T. Tsurutani, and V. M. Vasyliunas (1994), What is a geomagnetic storm?, *J. Geophys. Res.*, *99*, 5771–5792.

Greenspan, M. E., and D. C. Hamilton (2000), A test of the Dessler-Parker-Sckopke relation during magnetic storms, *J. Geophys. Res.*, *105*, 5419–5430.

Gussenhoven, M. S., D. A. Hardy, and W. J. Burke (1981), DMSP/F2 electron observations of equatorward boundaries and their relationship to the magnetospheric electric fields, *J. Geophys. Res.*, *86*, 768–778.

Hilmer, R. V., and G.-H. Voigt (1995), A magnetospheric magnetic field model with flexible driven by independent physical parameters, *J. Geophys. Res.*, *100*, 5613–5626.

Horwitz, J. L., S. Menteer, J. Turnley, J. L. Burch, J. D. Winningham, C. R. Chappel, J. D. Craven, L. A. Frank, and D. W. Slater (1986), Plasma boundaries in the inner magnetosphire, *J. Geophys. Res.*, *91*, 8861–8882.

Kamide, Y., et al. (1998), Current understanding of magnetic storms: Storm-substorm relationships, *J. Geophys. Res.*, *103*, 17,705–17,728.

Kauristie, K., J. Weygand, T. I. Pulkkinen, J. S. Murphree, and P. T. Newell (1999), Size of the auroral oval: UV ovals and precipitation boundaries compared, *J. Geophys. Res.*, *104*, 2321–2331.

Kozyra, J. U., M. W. Liemohn, C. R. Clauer, A. J. Ridley, M. F. Thomsen, J. E. Borovsky, J. L. Roeder, V. K. Jordanova, and W. D. Gonzalez (2002), Multistep *Dst* development and ring current composition changes during the 4–6 June 1991 magnetic storm, *J. Geophys. Res.*, *107*(A8), 1224, doi:10.1029/2001JA000023.

Kubyshkina, M. V., V. A. Sergeev, and T. I. Pulkkinen (1999), Hybrid input algorithm: An event- oriented magnetospheric model, *J. Geophys. Res.*, *104*, 24,977–24,993.

Le, G., C. T. Russell, and K. Takahashi (2004), Morphology of the ring current derived from magnetic field observation, *Ann. Geophys.*, *22*, 1267–1295.

Liemohn, M. W., J. U. Kozyra, C. R. Clauer, and A. J. Ridley (2001a), Computational analysis of the near-Earth magnetospheric current system during two-phase decay storms, *J. Geophys. Res.*, *106*, 29,531–29,542.

Liemohn, M. W., J. U. Kozyra, M. F. Thomsen, J. L. Roeder, G. Lu, J. E. Borovsky, and T. E. Cayton (2001b), Dominent role of the asymmetric ring current in producing the stormtime Dst*, *J. Geophys. Res.*, *106*, 10,883–10,904.

Lui, A. T. Y., and C. D. Anger (1973), A uniform belt of diffuse auroral emission seen by the ISIS-2 scanning photometer, *Planet. Space Sci.*, *21*, 799–810.

Maltsev, Y. P. (2004), Points of controversy in the study of magnetic storms, *Space Sci. Rev.*, *110*(3–4), 227–277.

Maltsev, Y. P., and A. A. Ostapenko (2001), The model of the magnetospheric magnetic field, *Geomagn. Aeron.*, *41*, 761–765.

Maltsev, Y. P., A. A. Arykov, E. G. Belova, B. B. Gvozdevsky, and V. V. Safargaleev (1996), Magnetic flux redistribution in the storm time magnetosphere, *J. Geophys. Res.*, *101*, 7697–7704.

McIlwain, C. E. (1986), A *Kp* dependent equatorial electric field model, *Adv. Space Res.*, *6*(3), 187–197.

Mead, G. D., and D. H. Fairfield (1975), A quantitative magnetospheric magnetic field model derived from spacecraft magnetometer data, *J. Geophys. Res.*, *80*, 523–534.

Meng, C.-I. (1978), Electron precipitations and polar aurora, *Space Sci. Rev.*, *22*, 223–300.

Meng, C.-I. (1983), Case studies of the storm time variation of the polar cusp, *J. Geophys. Res.*, *88*, 137–149.

Meng, C.-I. (1984), Dynamic variation of the auroral oval during intense magnetic storms, *J. Geophys. Res.*, *89*, 227–235.

Newell, P. T., and C.-I. Meng (1994), Ionospheric projections of magnetospheric regions under low and high solar wind pressure conditions, *J. Geophys. Res.*, *99*, 273–286.

Newell, P. T., Y. I. Feldstein, Y. I. Galperin, and C.-I. Meng (1996), The morphology of nightside precipitation, *J. Geophys. Res.*, *101*, 10,737–10,748.

Newell, P. T., V. A. Sergeev, G. R. Bikkuzina, and S. Wing (1998), Characterising the state of magnetosphere: testing the ion precipitation maxima latitude (b2i) and the ion isotropy boundary, *J. Geophys. Res.*, *103*, 4739–4745.

Newell, P. T., K. Liou, T. Sotirelis, and C.-I. Meng (2001), Polar Ultraviolet Imager observations of global auroral power as a function of polar size and magnetotail stretching, *J. Geophys. Res.*, *106*, 5895–5905.

Newell, P. T., T. Sotirelis, J. M. Ruohoniemi, J. F. Carbary, K. Lipu, J. P. Skura, C.-I. Meng, C. Deehr, D. Wilkinson, and F. J. Rich (2002), OVATION: Oval variation, assessment, tracking, intensity, and online nowcasting, *Ann. Geophys.*, *20*, 1039–1047.

Nishida, A. (1966), Formation of plasmapause, or magnetospheric plasma knee, by the combined action of magnetospheric convection and plasma escape from the tail, *J. Geophys. Res.*, *71*, 5669–5677.

Olson, W. P., and K. A. Pfitzer (1982), A dynamic model of the magnetospheric magnetic and electric fields for July 29, 1977, *J. Geophys. Res.*, *87*, 5943–5948.

Ostapenko, A. A., and Y. P. Maltsev (2000), Storm time variation in the magnetospheric magnetic field, *J. Geophys. Res.*, *105*, 311–316.

Papitashvili, V. O., F. J. Rich, M. H. Heinemann, and M. R. Hairston (1999), Parametrization of the DMSP ionospheric electrostatic potentials by the IMF strength and direction, *J. Geophys. Res.*, *104*, 177–184.

Pchelkin, V. V., Y. P. Maltsev, A. A. Ostapenko, and E. V. Pchelkina (2004), Distribution of electric currents in various magnetospheric models, paper presented at the 5th International Conference on Problems of Geocosmos, St. Petersburg Univ., St. Petersburg, Russia.

Rowland, D. E., and J. R. Wygant (1998), Dependence of the large-scale, inner magnetospheric electric field on geomagnetic activity, *J. Geophys. Res.*, *103*, 14,959–14,964.

Schoedel, R., K. Dierschke, W. Baumjohann, R. Nakamura, and T. Mukai (2002), The storm time central plasma sheet, *Ann. Geophys.*, *20*, 1737–1741.

Shue, J.-H., J. K. Chao, H. C. Fu, C. T. Russell, P. Song, K. K. Khurann, and H. J. Singer (1997), A new functional from to study the solar wind control the magnetopause size and shape, *J. Geophys. Res.*, *102*, 9497–9511.

Skoug, R. M., et al. (2003), Tail-dominated storm main phase: 31 March 2001, *J. Geophys. Res.*, *108*(A6), 1259, doi:10.1029/2002JA009705.

Starkov, G. V., B. V. Rezhenov, V. G. Vorobjev, Y. I. Feldstein, and L. I. Gromova (2002), Auroral precipitations structure in the daytime sector (in Russian), *Geomagn. Aeron.*, *42*(2), 186–194.

Starkov, G. V., B. V. Rezjenov, V. G. Vorobjev, and Y. I. Feldstein (2003), Planetary distribution of the auroral precipitations ant their relation with auroral region luminosity (in Russian), *Geomagn. Aeron.*, *43*(5), 609–619.

Tsyganenko, N. A. (1987), Global quantitative models of the geomagnetic field in the cislunar magnetosphere for different disturbance level, *Planet. Space Sci.*, *35*, 1347–1358.

Tsyganenko, N. A. (1989), A magnetospheric magnetic field model with a warped tail current sheet, *Planet. Space Sci.*, *37*, 5–20.

Tsyganenko, N. A. (1995), Modeling the Earth's magnetospheric magnetic field confined within a realistic magnetopause, *J. Geophys. Res.*, *100*, 5599–5612.

Tsyganenko, N. A. (1996), Effects of the solar wind conditions on the global magnetospheric configurations as deduced from data-based field models, in *Proceedings of 3rd International Conference on Substorms*, *Versailles, France, ESA SP-389*, pp. 181–185, Eur. Space Agency, Paris.

Tsyganenko, N. A. (2002), A model of the near magnetosphere with a dawn-dusk asymmetry: 2. Parametrization and fitting to observations, *J. Geophys. Res.*, *107*(A8), 1176, doi:10.1029/2001JA000220.

Tsyganenko, N. A., G. Le, C. T. Russell, and T. Iyemori (1999), A study of the inner magnetosphere based on data of Polar, *J. Geophys. Res.*, *104*, 10,275–10,283.

Tsyganenko, N. A., H. J. Singer, and J. C. Kasper (2003), Storm-time distortions of the inner magnetosphere: How severe can they get, *J. Geophys. Res.*, *108*(A5), 1209, doi:10.1029/2002JA009808.

Turner, N. E., D. N. Baker, T. I. Pulkkinen, and R. L. McPherron (2000), Evaluation of the tail current contribution to *Dst*, *J. Geophys. Res.*, *105*, 5431–5439.

Turner, N. E., D. N. Baker, T. I. Pulkkinen, J. I. Roeder, J. F. Fennell, and V. K. Jordanova (2001), Energy content in the storm time ring current, *J. Geophys. Res.*, *106*, 19,149–19,156.

Turner, N. E., T. I. Pulkkinen, D. N. Baker, and R. L. McPherron (2002), Reply, *J. Geophys. Res.*, *107*(A1), 1011, doi:10.1029/2001JA900099.

Vorobjev, V. G., L. I. Gromova, B. V. Rezhenov, G. V. Starkov, and Y. I. Feldstein (2000), The boundaries of plasma precipitation and auroral luminosity positions in night sector (in Russian), *Geomagn. Aeron.*, *40*(3), 79–85.

I. I. Alexeev, Institute of Nuclear Physics, Moscow University, 119899, Moscow, Russia. (alexeev@dec1.npi.msu.su)

L. Alperovich, Department of Geophysics and Planetary Sciences, Tel Aviv University, 69978 Tel Aviv, Israel. (leonid@frodo.tau.ac.il)

L. A. Dremukhina, Y. I. Feldstein, L. I. Gromova, and A. E. Levitin, Institute of Terrestrial Magnetism, Ionosphere and Radio Wave Propagation, 142190 Troitsk, Moscow Region, Russia. (aifeld@aol.com; lgromova@izmiran.troitsk.ru; aelevitin@yandex.ru)

W. D. Gonzalez, Istituto de Pesquisas Especiais, 12201-970 Sao Jose dos Campos, Sao Paulo, Brazil. (gonzalez@dge.inpe.br)

J. U. Kozyra, Space Physics Research Laboratory, University of Michigan, 2455 Hayward, Ann Arbor, MI 48109, USA. (jukozyra@engin.umich.edu)

U. Mall, Max Planck Institute for Aeronomy, Katlenburg-Lindau, D-37191 Germany. (mall@linmpi.mpg.de)

B. T. Tsurutani, Jet Propulsion Laboratory, Pasadena, CA 9109, USA. (btsurutani@jplsp.jpl.nasa.gov)

A. Prigancova, Geophysical Institute, Slovak Academy of Sciences, 845 28 Bratislava, Slovakia. (geofpria@savba.sk)

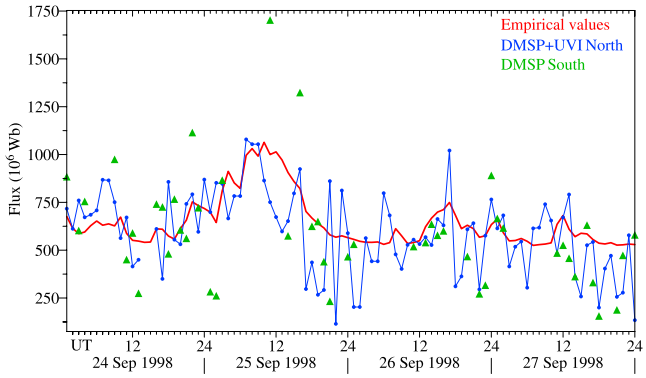

Figure 6. Variations of the magnetic flux from the polar cap calculated using empirical equations (2), (3), (6), and (7) (solid line), the magnetic flux calculated using the POLAR UV photometer and DMSP particles measurements in the northern hemisphere (DMSP + UVI North: solid line), and DMSP particles measurements in the southern hemisphere (DMSP South: triangles) during the 24–27 September 1998 magnetic storm. The OVATION method is used to obtain the DMSP + UVI North and DMSP South values.